E.C. van der Veer
4220781

Correlation and modelling of a fluvial depositional system

Outcrop analogue study of thin-bedded fluvial reservoir sandstone

TU Delft

Correlation and modelling of a fluvial depositional system

Outcrop analogue study of thin-bedded fluvial reservoir sandstone

By

E.C. van der Veer

in partial fulfilment of the requirements for the degree of

Bachelor of Science
in Applied Earth Sciences

at the Delft University of Technology,
to be defended publicly on Wednesday, 15th of June at 14:00 AM.

Daily supervisor: Dr. M.E. Donselaar
Supervisors: Dr. K.H.A.A. Wolf
K.A. van Toorenenburg

TU Delft

Abstract

The Huesca fluvial fan contains a low gradient fluvial system with well-exposed, 3D outcrops. An outcrop study of low-sinuous deposits aims to provide a deterministic reservoir model that predicts correlation lengths, nesting and reservoir potential of thin-bedded fluvial reservoir sandstone in an overall low net-to-gross setting. To correlate the study area, centimetre accurate dGPS measurements of paleosols have been collected to calculate the tectonic dip. This was used to correlate lithostratigraphic logs of the area. Correlation lengths between wells are dependent on how spatial and continuous a paleosol has developed. Photo panels of the outcrop were analysed for net-to-gross ratio and distribution of channel and floodplain deposits. A clear distinction between high and low net-to-gross regions can be observed in the panels, which causes a lateral heterogeneity. This can be explained by the nesting of a river channel. Nesting can be caused by local avulsions triggered by crevasse splays of the river channel in combination with avulsion by annexation. The lateral heterogeneous character can have major implications on reservoir potential. The reservoir volume is dependent on the connectivity between the higher and lower net-to-gross regions. The heterogeneity also has an impact on reservoir modelling as there only is a limited subsurface expression from wells. Therefore, it cannot be known whether the higher or lower net-to-gross zones are being looked at for that particular fluvial system which makes estimates about reservoir volume difficult and inaccurate.

Acknowledgements

This thesis is part of the tough gas research project supported by EBN and Engie. The Molengraaff fund kindly awarded me a grant for the fieldwork.
I want to thank my supervisor Rick Donselaar for allowing me to be a part of this research and for the excellent guidance both in the field and during processing. I also want to thank Koen van Toorenenburg who has helped and guided me through this project. I want to thank Thore Boerboom and Axel Sanden for the weeks in the field, kindly providing the logs and sparring sessions about interpretations of data.

Contents

1. Introduction

Now that conventional reservoirs in mature areas are reaching the end of their life, tight gas reservoirs are gaining importance as potential secondary hydrocarbon reservoirs. One of the focus areas of tight gas exploration in NW Europe is on previously by-passed stratigraphic intervals of fluvial origin that surround existing infrastructure. These thin-bedded fluvial sandstones have been interpreted as lobate crevasse-splay deposits, which may be connected to fluvial channel sandstone (Donselaar et al., 2015).To understand the reservoir architecture of such low net to gross deposits, a detailed knowledge of depositional mechanisms, facies interrelationships, reservoir geometry, stacking and amalgamation patterns, connectivity, and the distribution of petrophysical properties is needed.

Ongoing research in modern-day fluvial systems shows that crevasse splays form lobes of sand deposits originating from a breach point in the levee of the river channel. The surface area of these sand beds may reach up to several square kilometres with a thickness ranging from centimetres to decimetres. (Toorenenburg et al., 2015) Crevasse splays fill up the floodplain by compensational stacking, forming amalgamated deposits with sand-on-sand connectivity. (Li et al., 2014) This results in stacked sand deposits. Despite the small thickness of individual crevasse splays, the surface area of the deposits results in an extensive net reservoir volume, especially when vertically stacked and interconnected crevasse splays occur.

Intervals of stacked crevasse splays can be identified on well-logs and cores (Donselaar & Schmidt, 2005) and are associated with aggradation of the fluvial system. When considering the total stratigraphy of the subsurface, channel deposits can be rare and therefore direct penetrations are limited. For this reason, outcrop analogue studies are performed to gain more insights by linking contemporary systems to the limited subsurface expression in wells.

The endorheic Ebro Basin in the NE of Spain provides a suitable outcrop analogue of a low-net-to-gross fluvial stratigraphy (Fig. 1.1). Previous outcrop studies have focused on reservoir characterization but existing facies correlations within this project are limited to channel belt scale. This project aims to expand the correlation to a sub-system scale, investigating multiple channel belts to find their hierarchy in time and space in relation to the occurrence of thin-bedded crevasse splay deposits.

To be able to make such correlation, a two-week field campaign was carried out at various outcrop localities in the Huesca fluvial fan. During the field campaign a data was gathered by taking photographs and centimetre-accurate differential-GPS (d-GPS) marker points of the Marcén ridge outcrop. The data is used for stereographic projections

Fig. 1.1: *The Marcén ridge outcrop of the Huesca fluvial fan (panel A continues into panel B; total length of 2.25 km, 150m high). There is a clear variation in net-to-gross ratio at various points in the outcrop.*

using specialized software. The result is a geo-referenced three-dimensional model of the studied outcrop. Together with field observations, the model serves as a basis for a large-scale correlation and interpretation of the facies associations in the fluvial system. This study aims to provide input for a deterministic reservoir architecture model that is well-constrained in space and, hence, has a very low uncertainty. The model serves to predict correlation lengths, nesting and reservoir potential of thin-bedded fluvial reservoir sandstone in an overall low net-to-gross setting.

2. Geological Setting

The fluvial system in this study forms a part of the Ebro Basin situated in Northern Spain. The basin formed as a foreland basin in the Pyrenean orogenic belt, which is a Cenozoic mountain belt, located on the boundary between the Iberian and Eurasian plate. (ECORS-Pyrenees Team, 1988) The Pyrenees are a part of the Alpine orogenic belt, and are a result of convergence between the Iberian sub-plate and the European plate during the Latest Cretaceous and Tertiary. (Lloyd et al.,1998) The first Pyrenean thrust sheets developed during the Late Cretaceous as a result of reactivation of Lower Cretaceous extensional faults. (Puigdefàbregas. et al., 1992) The South Pyrenean Zone is situated on the southern side of the Pyrenees and is separated from the Ebro Basin by the External Sierras, also called the Sierras Marginales. (Lloyd, M.J. et al.,1998) (Fig. 2.1) The Sierras Marginales are east-west oriented and are the southernmost thrust front. These developed under NNE-SSW compression during the Late Cretaceous and Miocene. (Puigdefàbregas, et al., 1992) The thrust sheet was a blind thrust until the Oligocene, from then on it formed a topographic high on the northern margin of the Ebro Basin. The Oligocene to Miocene alluvial sediments in the Ebro Basin are largely undeformed, with the exception of the deposits immediately at the rim of the thrust front due to continued thrusting during deposition and salt tectonics near Barbastro. (Lloyd et al.,1998)

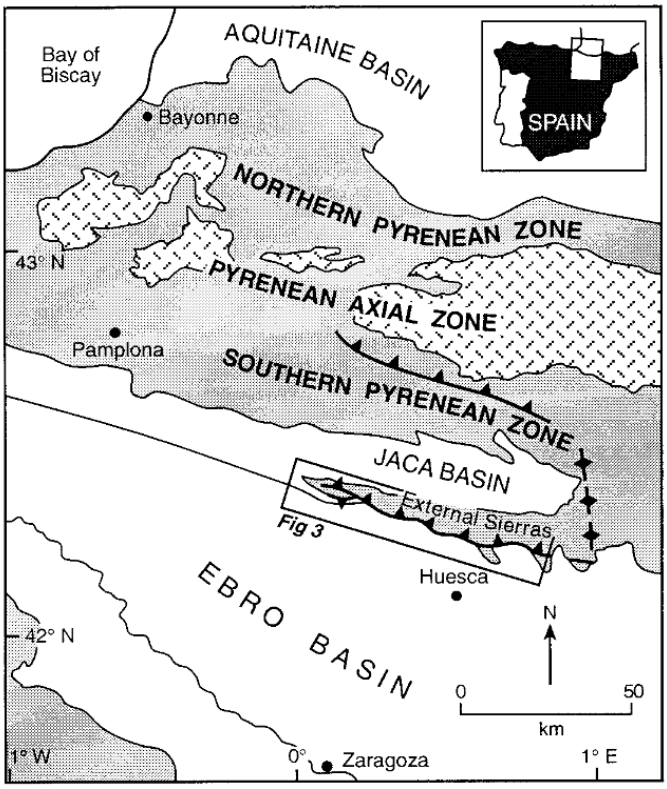

Fig. 2.1: *Location of the southern western part of the Pyrenees and the adjacent Ebro Basin in Northern Spain. From Lloyd et al.,1998*

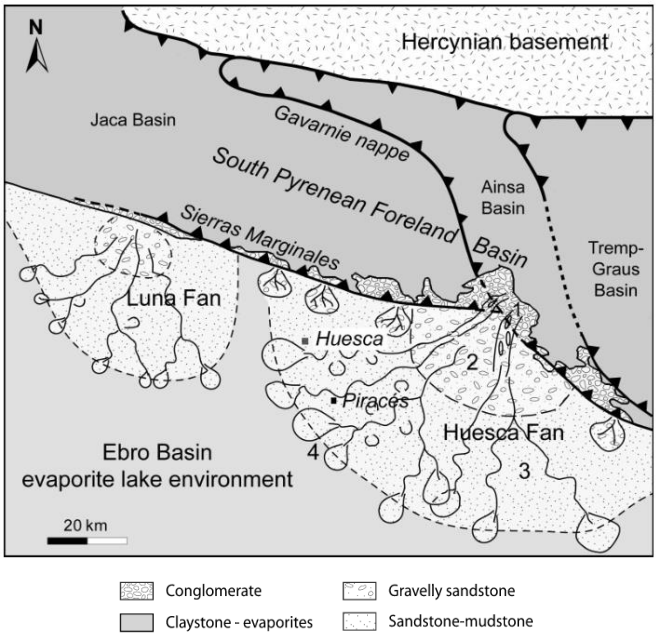

Fig. 2.2: *Facies distribution of the Huesca fluvial fan. (1), line source apex with confined conglomerate-filled paleo-valleys in folded and faulted Eocene limestone of the Sierras Marginales; (2), open braid plain; (3), distal fan area with meander belts in a floodplain; (4), fan fringe: small meandering rivers end in terminal lobes and sheets. Modified from Hirst & Nichols (1986) and Munoz (1992). From Donselaar & Schmidt, 2005.*

The study area is part of the Huesca Fluvial Fan, which is situated at the Northern rim of the Ebro Basin. (Fig. 2.2) Sediment was derived from the Pyrenean mountain and the South Pyrenean Foreland Basin. The apex of the Huesca Fluvial Fan is a fractured zone in the Sierras Marginales thrust front. Next to the Huesca fan, the smaller Luna fan was deposited. (Fig. 2.2) Both fluvial systems drained into the lacustrine system in the centre of the land-locked Ebro Basin. The lake was the regional base level. (Donselaar & Schmidt, 2005) The fluvial systems are described as fluvial distributary systems that are characterized by their radial pattern of channels from the apex. They also show typical decrease in channel size downstream, decrease in grainsize downstream and lack of lateral confinement. (Nichols & Fisher, 2007)

As seen in Fig. 2.1 the paleo currents show a radial pattern with a trend to the northwest along the thrust sheet of the Sierras Marginales. (Hirst, 1992) From the apex to the distal part of the Huesca fan the average grain size is fining, with massive braided stream conglomerates filling the paleo valleys in the apical zone. At the proximal part of the fan, braided river deposits formed gravelly sandstone beds that amalgamated to

extensive sheets with associated overbank siltstone deposits. Looking toward the lake margin, the sandstone-to-siltstone proportion decreases and meandering river sandstone deposits become the dominant lithology. The sandstones are thin and fine grained and embedded in extensive floodplain deposits. Still further distal, at the rim of the Huesca fan, the fluvial deposits dominantly consist of siltstone and claystone with thin, ribbon or sheet-shaped sandstone bodies. (Donselaar & Overeem, 2008)

The paleoclimate for the Huesca fan region was found to be similar to the current climate. It is characterized as a seasonal subtropical and humid region with an annual mean of 14˚C. (Weltje, 1996; Donselaar & Overeem, 2008) Based on the development of paleosols and microfossils, the climate is interpreted as humid. A changing lake level indicates an alternating arid and wet climate, resulting in evaporites and limestone deposits. (Donselaar and Overeem, 2008)

3. Data and Methods

This study is based on data gathered during a field campaign in the north-east of Spain. This field campaign was carried out in April 2016 in the Huesca Fluvial Fan. The fieldwork was done in the region of the village of Marcén, with the primary location being the Marcén ridge. This outcrop of low-sinuous channel deposits is well exposed and provides 2.25km of 150m cliff faces. Amphitheatre-shaped incisions in the ridge add to the exposure of the channel belt deposits, giving a (pseudo) 3D view of the fluvial system. A well-developed paleosol can be found in the ridge, which is shown in Fig. 3.1. Access to the higher parts of the outcrop is limited due to scree and steep slopes.

Fig. 3.1: *View of the Marcén ridge. The amphitheater shaped incision and the steep cliff faces can be seen. The yellow arrows indicate the well-developed red and grey paleosol.*

The second location used for this study consists of three buttes located approximately 1.2km to the south of the Marcén ridge. The buttes are approximately 50m wide and are approximately 50m high. The buttes provide a 360 degrees 3D perspective of the fluvial strata. Access to some parts of the buttes is limited due to steep cliff faces and scree. Locations are shown in Fig. 3.3. A photo panel of the Marcén ridge can be seen in Fig. 1.1 and a view of the three buttes can be seen in Fig. 3.4.

3.1 Data acquisition

During the field campaign lithostratigraphic logs were taken on a 1:50 scale. Field campaigns in previous years resulted in lithostratigraphic logs on a 1:50 scale of butte 1 and 2. In these logs grain size, lithology, colour, bioturbation, sedimentary structures, flow directions, thickness, and contacts were noted. (appendix B (fig 3.2)) A geological hammer, compass, measuring tapes, a hand lens and a grain size ruler, Garmin GPSmap 60 CSx device and a Nikon laser range finder were used to obtain the data for the logs. The locations of the logs can be found in Fig. 3.5. Photo panels of the Marcén ridge were made with a Nikon D300 camera. These panels were used in the field to indicate the dGPS markers.

Fig. 3.2: *Legend for the sedimentary structures in the lithostratigraphic logs.*

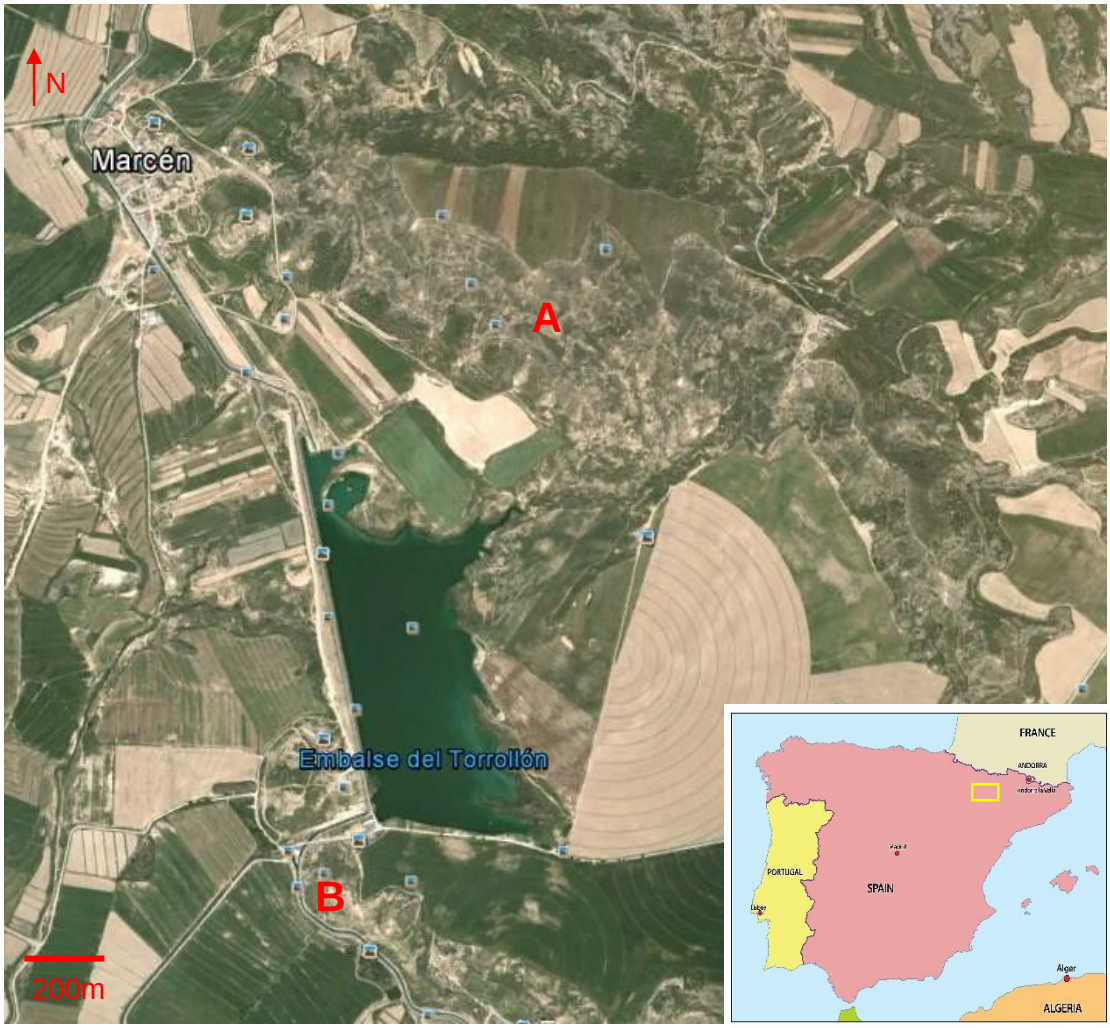

Fig. 3.3: *Location of the study area in the Huesca Fluvial Fan. The satellite picture shows the studied outcrop, with the town of Marcén in the top left. 'A' indicates the Marcén ridge and 'B' indicate the buttes studied in previous years. Images retrieved from Google Earth (20/05/2016).*

Fig. 3.4: *View of the three buttes from the Marcén ridge. Butte 1&2 are approximately 50m wide.*

Fig. 3.5: *Locations of the lithostratigraphic logs. Image retrieved from Google Earth (24/05/2016).*

3.1.1 Differential GPS

Accurate GPS data is needed for correlating the sandstone channels and floodplain deposits. As this study is undertaken in an area with an expected tectonic dip that is very low, this dip can only be determined with accurate GPS measurements. GPS devices normally provide spatial data with an accuracy of 3-5m in lateral directions, and height measurements with an even greater error. For this study more precise data is needed to be able to correlate this area. This accurate spatial data was obtained with a Trimble R7 differential GPS (dGPS) unit.

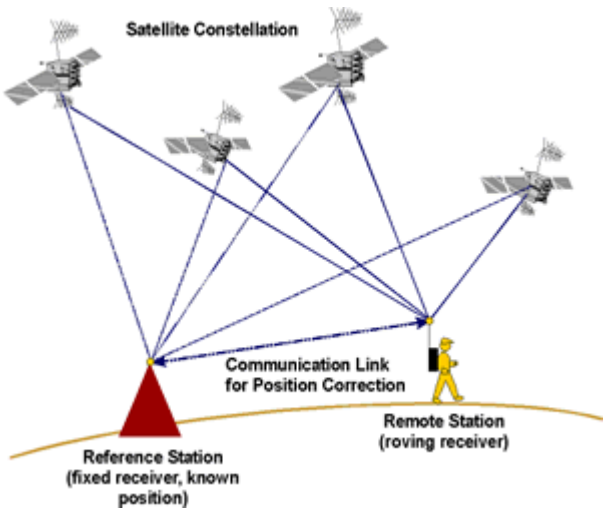

Fig. 3.6: *Differential GPS set up. The fixed receiver measures the timing error of the signal and provides a correction for the roving receiver. This results in an error of only a few centimeters*.

The underlying basis of dGPS is that two receivers will experience comparable atmospheric errors when they are close to each other. GPS measurements are inflicted with errors due to inconsistencies of atmospheric conditions that affect the speed of the GPS signal as it passes through the Earth's atmosphere. The dGPS therefore requires two receivers operated at the same time, a reference station that measures the timing errors and provides correction for the remote station. (Fig. 3.6) This reduces the error of the measurements of the remote station to a max of five centimetres. The reference station is set op on a fixed position for all surveying sessions and the remote station is taken into the field and positioned on places of interest.

3.1.2 Geo referencing

To be able to geo reference the logs, but also to correlate the area, geographic data was gathered using a Trimble R7 differential GPS unit. The data of the Mogache geodetic triangulation point was used to check the accuracy of the dGPS unit. The data that belongs to the geodetic point was retrieved from the Instituto Geográfico Nacional (IGN). The dGPS gives data output in the WGS84 latitude and longitude coordinate system and WGS84 ellipsoid for vertical datum. The IGN gives output in the ETRS89 coordinate system. The difference between the data is shown in Table 3.1 and is caused by the use of local (ETRS89) and a global (WGS84) coordinate system.

Table 3. 1: *Coordinates of the Mogache geodetic point measured by the dGPS and the data from IGN. Coordinates are expressed in degree, minute, second form. Elevation is based on the mean sea level at Alicante.*

	Latitude	***Longitude***	***Elevation (m)***
Geodetical point dGPS (dms)	41 93 21.57 N	02 72 10.3277 W	591.651
Geodetical point IGN (dms)	41 93 21.47 N	02 72 11.5847 W	590.331
Difference (dms)	00 00 00.10 N	00 00 01.2570 W	1.320
Difference (m)	1.0	1.1	1.320

3.2 Data processing

3.2.1 Calculating tectonic dip

The tectonic dip in the area studied during the field campaign is very low. For the Huesca Fluvial Fan a maximum of 2˚ is described in literature (Hirst,1992). This dip is not possible to measure with a compass because a geological compass has a reading error of 2˚. This means dGPS data can be used to more accurately determine the tectonic dip and azimuth. The data obtained from the surveys with the dGPS is used to calculate a least squares solution for a plane that fits best through the data-points. To perform this calculation, the dGPS data is converted from WGS84 to the ETRS89 UTM 30N coordinate system and is fit to equation 3.1.

$$\boldsymbol{z} = N_E\boldsymbol{u} + N_N\boldsymbol{v} + N_v \tag{3.1}$$

where **z** = elevation, **u** = UTM Easting coordinates and **v** = UTM Northing coordinates. The values for N are calculated with equation 3.2.

$$\widehat{N} = (X^T X)^{-1} X^T \boldsymbol{z} \;\; with\, \widehat{N} = \begin{pmatrix} N_v \\ N_E \\ N_N \end{pmatrix} \; and\; X = \begin{pmatrix} 1 & u_1 & v_1 \\ \vdots & \vdots & \vdots \\ 1 & u_n & v_n \end{pmatrix} \tag{3.2}$$

The calculations were done in Microsoft Excel using the LINEST function.

The vector $\widehat{N}$ is the normal vector of the plane and can be used to calculate the dip (δ) with equation 3.3 and the direction of the normal vector (θ) with equation 3.4.

$$\delta = tan^{-1}\left(\frac{N_N}{N_E}\right) \tag{3.3}$$

$$\theta = tan^{-1}\left(\frac{\sqrt{N_N^2+N_E^2}}{N_v}\right) \tag{3.4}$$

The results for the dip have to be multiplied by 180/π to convert from radians to degrees. The azimuth is calculated from the results of equation 3.4 by adding 90˚ to the strike to calculate the azimuth and adding another 180˚ to get the dipping direction instead of the upward direction.

To determine the accuracy of the tectonic dip a sensitivity analysis was performed on the data. This was done by taking 6-10 data points and calculating the dip and azimuth with them. This action was performed 40 times on randomly selected data points and the results were divided into bins. To get a graphical representation of the result of the sensitivity analysis the bins were plotted in histograms.

3.2.2 Stereographic projection

The photo panels taken at the Marcén ridge were used to create a 3D model of the ridge. This was done with Agisoft Photoscan, which is software that performs photogrammetric processing of digital images and generates 3D spatial data. The theory behind the creation of 3D models from 2D images is triangulation. The principle of this process is that there is a relationship between multiple views which convey information about corresponding sets of points which must contain some structure. This structure is related to the position and the calibration of the camera. Figure 3.7 illustrates the principle of triangulation. In this figure p_l and p_r are corresponding points on two photographs that have to be triangulated to determine the depth in the 3D model. The stereo triangulation problem consists of retrieving the 3D coordinates P_l and P_r from the image coordinates p_l and p_r. This can be determined with the following camera parameters: focal length, image sensor format, principal point camera position and lens distortion of the camera. This corresponds to point P, which is the intersection between the two arrays (O_l, p_l) and (O_r,p_r). (Li et al., 2011)

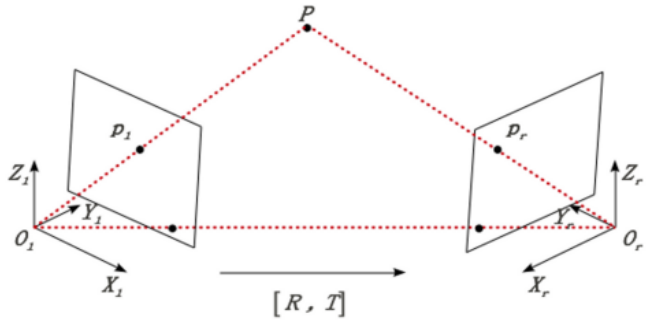

Fig. 3.7: *p_l and p_r are corresponding points on two photographs that have to be triangulated to determine the depth in the 3D model. The stereo triangulation problem consists of retrieving the 3D coordinates P_l and P_r from the image coordinates p_l and p_r. This can be calculated with the parameters of the camera. This corresponds to point P, which is the intersection between the two arrays (O_l, p_l) and (O_r,p_r). From Li et al., 2011*

The software Agisoft Photoscan has a workflow that guides you through the process of building a 3D model. The program has to align the photos and for this process the user has to mask the parts of the photo's that are not important. These unimportant parts are the regions in the photo that are occupied by air, vegetation and other objects that are not the outcrop. The user also has to place markers on the photos to guide the program in the process. These markers are dGPS points of recognizable objects or positions on the ridge.

The coordinates from the dGPS markers are also given as input for the model, which gives the software information about the dimensions of the Marcén ridge and is therefore able to georeferenced the model.

3.2.3 Correlating fluvial deposits

To be able to correlate the area, the dip and azimuth have to be known to make it possible to correlate the fluvial deposits. Paleosols in between layers can be used to correlate because a paleosol represents a lengthy duration of absence of sediment influx. The development of paleosols is influenced by the rate and continuity of sediment accumulation and consequently paleosols can help to correlate and interpret sediment deposition. The spatial distribution of paleosols reflects the landforms on which they formed and the processes operating in the depositional environment. (Kraus, 1999) A paleosol therefore gives an indication of the tectonic dip at the time of deposition. With the method described in 3.2.1 the normal vector of the plane can be calculated.

The logs can be correlated by calculating the expected height in the different log locations with the normal vector resulting from the least squares solution. This can be done by using the ETRS89 coordinates as a location on the corresponding plane and this will give the expected height in the logs. These heights will then be compared with the logs to see if there are corresponding layers in the different logs that correlate.

The dip and azimuth are necessary to correlate the Marcén ridge and the buttes but also to correlate fluvial deposits in the Marcén ridge. The 3D model is used to connect the sandstone bodies by plotting the calculated plane resulting from the paleosol through the corresponding layers as this corresponds to the correct dip and azimuth of the ridge. To show which sandstone bodies connect, Adobe Illustrator is used to put overlays over corresponding layers.

4. Results

4.1 Paleosols

To be able to use the paleosols for correlating the area, the tectonic dip and azimuth are needed. The calculation methods described in chapter 3.2.1 were used to calculate these values for the paleosols distinguished in the Marcén ridge. The results are presented in Table 4.1
Paleosol 1 is a Bordeaux red paleosol situated on the bottommost position in a succession of four paleosols. It is exposed in the base of the Marcén ridge. Paleosol Butte 2 is also part of a series of four paleosols and is also found as the lowest paleosol. Paleosol 2 and 1 can be observed in the Marcén ridge. Paleosol 2 is exposed in the NNW part of the ridge near the village of Marcén and has a red base with a blueish grey top. Paleosol 1 can be seen in the middle of the ridge near log 6 and 4 and is characterized by its grey top and brick red base. The combined paleosol is a combination between paleosol 1 and the paleosol in butte 2. This combination was made due to the matching features which indicated that the paleosols were the same.

Table 4.1: *Results of the calculation of the tectonic dip and azimuth for different paleosols and combinations. N represents the number of dGPS data points and R^2 is the coefficient of determination. It compares estimated and actual y-values, and ranges in value from 0 to 1. If it is 1, there is a perfect correlation in the sample.*

	Paleosol 3	***Paleosol 2***	***Paleosol 1***	***Paleosol Butte 2***	***Combined paleosol***
N (-)	38	10	6	18	23
Azimuth (˚)	268.16	311.33	352.00	302.53	269.11
Dip (˚)	0.47	0.29	0.53	0.53	0.57
R^2 (-)	0.99	0.94	0.53	1.00	0.98

To be able to compare the accuracy of the calculated tectonic dip the coefficient of determination, R^2 is used. This value compares estimated and actual y-values, and ranges in value from 0 to 1. If it is 1, there is a perfect correlation in the sample. Paleosol 1 has a very low R^2 value, and only 6 data points. Because of the low R^2 value this paleosol on its own is left out for further correlation because it is not accurate and reliable enough. However, from observations in the field it was expected that paleosol 1 would correlate with the paleosol in butte 2 so these values were combined and fitted together. This fit gave an azimuth and dip of 269/0.57 and a high R^2 value. This is option one for the orientation and dip in the lower parts of the Marcén ridge and buttes. The second option is that the azimuth and dip of 302/0.53 of the paleosol in butte 2 are true for the lower parts of the area. For the higher parts of the ridge, the tectonic dip of paleosol 3 is chosen.

The results of the sensitivity analysis performed on paleosol 3, paleosol butte 2 and the combined paleosol are presented in Fig. 4.1 and 4.2. Looking at the histograms of paleosol 3 and butte 2 it can be observed that the values for both the azimuth and dip are constant and therefore the values in Table 4.1 are reliable.

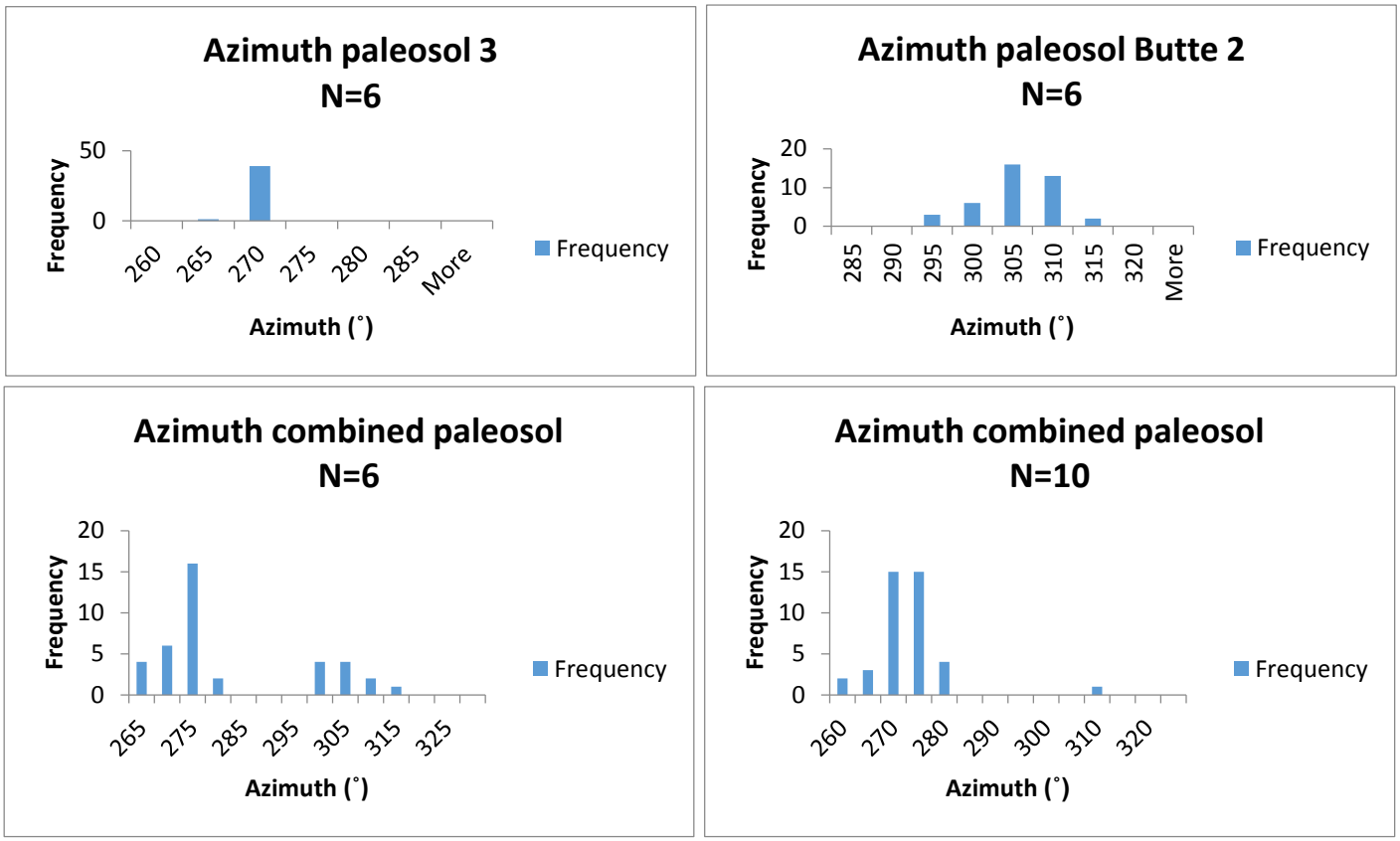

Fig. 4.1: *Histograms of the sensitivity analysis of the azimuth of the paleosols. Bin sizes are of equal width and were determined by creating equal intervals between the minimum and maximum value.*

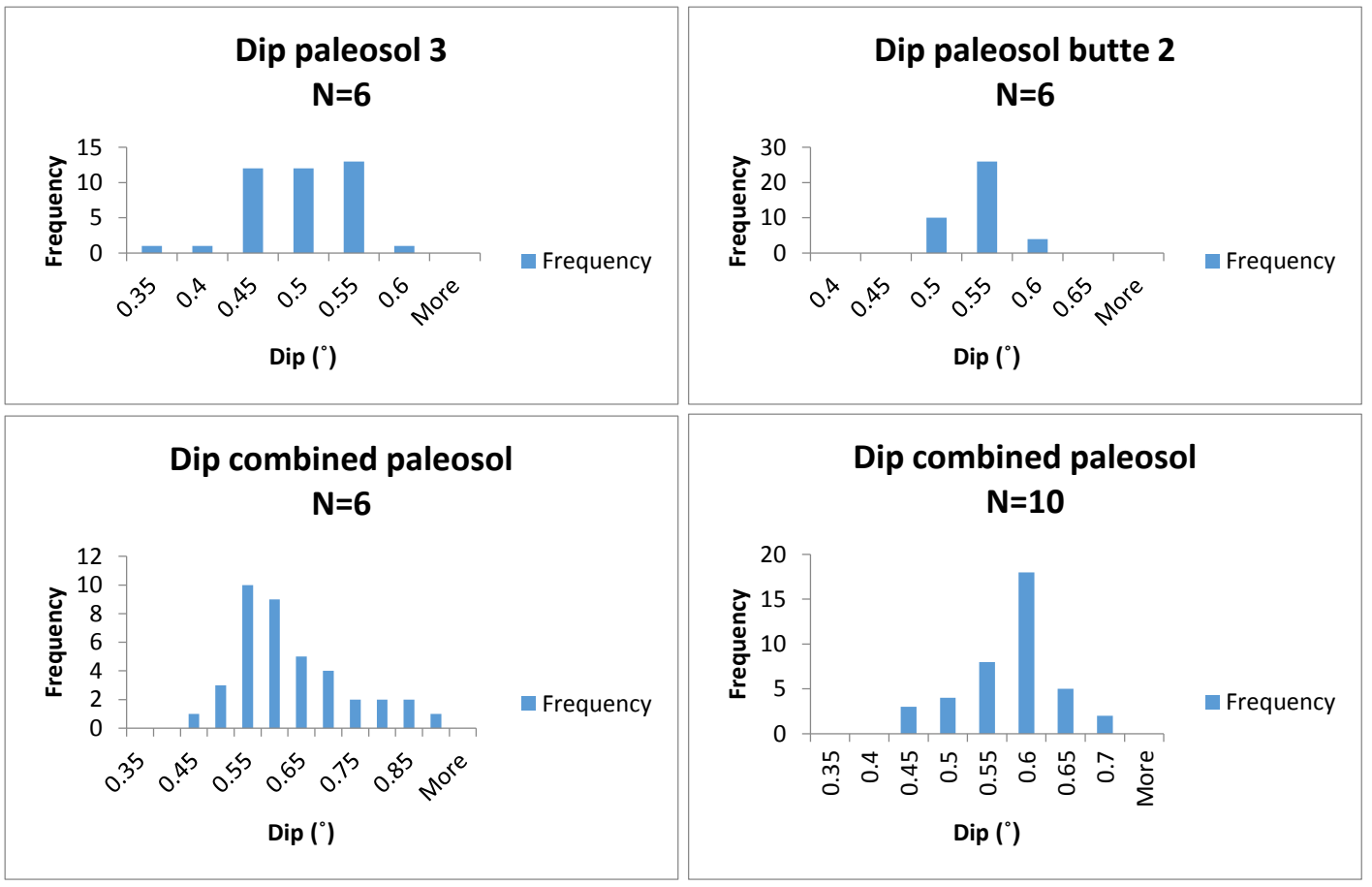

Fig. 4.2: *Histograms of the sensitivity analysis of the dip of the paleosols. Bin sizes are of equal width and were determined by creating equal intervals between the minimum and maximum value.*

The expected heights of the paleosols in the different logs are presented in Table 4.2. Looking at Fig 4.4, the expected heights of paleosol 3 can all be found in the logs which means this azimuth and dip can be used in the vicinity of this paleosol. Fig. 4.4 shows part of the logs with the values for paleosol 3 represented by the blue line. For the lower parts of the area both options are presented in the logs in Fig. 4.5 and 4.6. Looking at the logs in Fig. 4.6 it can be seen that the expected heights of option 2 do not correspond to the heights of the paleosol. Option 1 however, shows that the heights in the logs agree with the expected heights so this option is used to correlate the lower parts of the area.

Table 4.2: *The expected and measured heights of the paleosols in the different logs.*

	Upper region Marcén ridge		***Lower region Marcén ridge***		
			Option 1	**Option 2**	
	Paleosol 3 (m)		**Combined paleosol (m)**	**Paleosol Butte 2 (m)**	
	Expected	*Measured*	*Expected*	*Expected*	*Measured*
Log 6	457.49	457.10	433.30	425.36	-
Log 4	460.11	459.57	436.44	427.71	-
Butte 1	457.98	457.85	434.16	434.53	-
Butte 2	453.08	452.83	429.28	428.21	428.22
Base Marcén ridge	-	-	432.90	425.98	432.72

4.2 Log correlation

With the azimuth and dip of the area known, the logs in Fig. 4.4 and 4.5 can be correlated. Starting at the bottom of the sequence in figure 4.5, sand bodies can be correlated with the help of the three paleosols above the yellow line representing the combined paleosol. As a paleosol represents a lengthy duration of absence of sediment influx in the area, the deposits underneath a paleosol originate from the same period of deposition before the duration of stability. As this system is low sinuous, flow directions were also used to correlate the area by predicting the direction of the main channel. In Fig. 4.5 the general flow direction of the main channel is SSW. Looking at the positions of the lithostratigraphic logs in Fig. 3.5 it is expected that a channel sand body in the Base Marcén ridge log will match a sand body in butte 2 since they are positioned on a SSW direction in respect to each other. Floodplain deposits are therefore expected in butte 1. At the heights 446m and 450m in butte 1 two thick sands are visible. At the corresponding heights in butte 2 thinner sand layers are found that can be interpreted as floodplain deposits or crevasse splays. The thinner sands have a measured orientation of 190˚ and because crevasse splays are oriented approximately 90˚ on the main channel the deposits in the logs can be linked. (Fig. 4.3) The main channel flow direction can also be predicted with this information and would result in a NNE - SSW orientation. This corresponds to the measured flow directions of the main channel in lower parts of the logs.

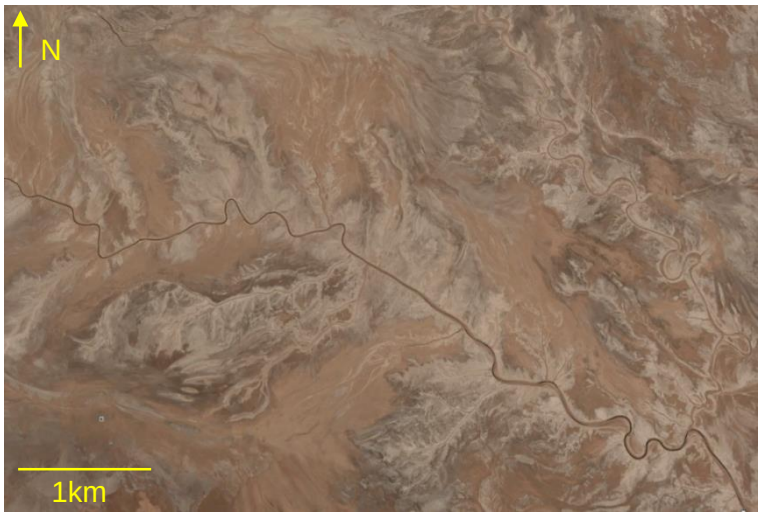

Fig. 4.3: *Example of a river system near Uyuni, Bolivia. The darker line is the main channel with the lighter coloured crevasse splays emerging from this channel. The crevasse splays approximately have a 90˚ orientation relative to the main channel. Image retrieved from Google Earth (2/6/2016).*

For the higher parts of the sequence the logs in Fig. 4.4 are used and are levelled at paleosol 3. These logs are more difficult to correlate because there are less well developed paleosols and less flow directions known. This made it difficult to make correlations between the buttes and log 4 and 6. Two correlations between the four logs were made based on flow directions of the two thick sands in the uppermost region of the logs. (Fig. 4.4)

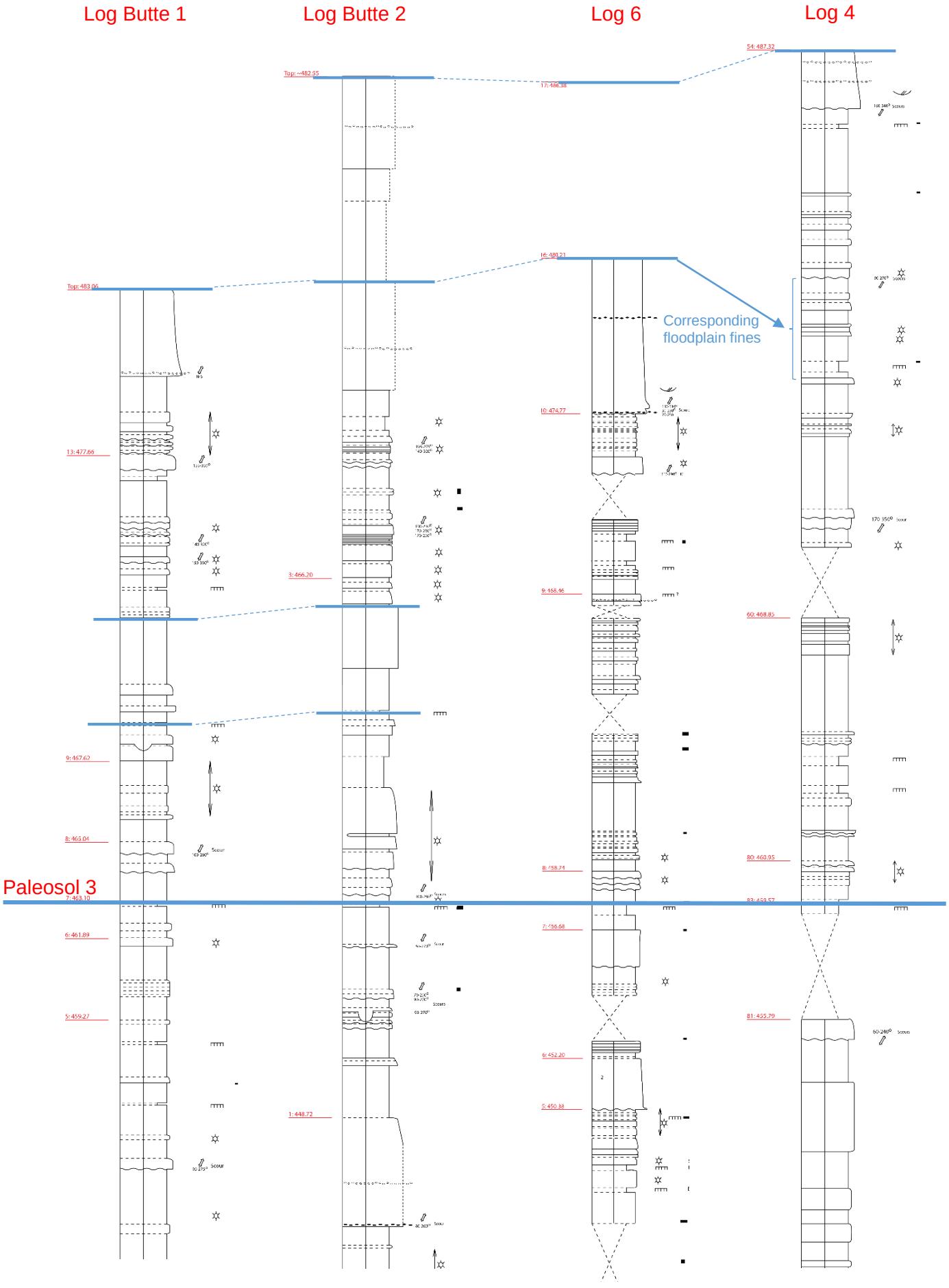

Fig. 4.4: *Log 6&4 and the logs from butte 1&2 levelled at the expected height of paleosol 3. An azimuth of 268˚ and a dip of 0.47˚ was used to calculate the expected heights.*

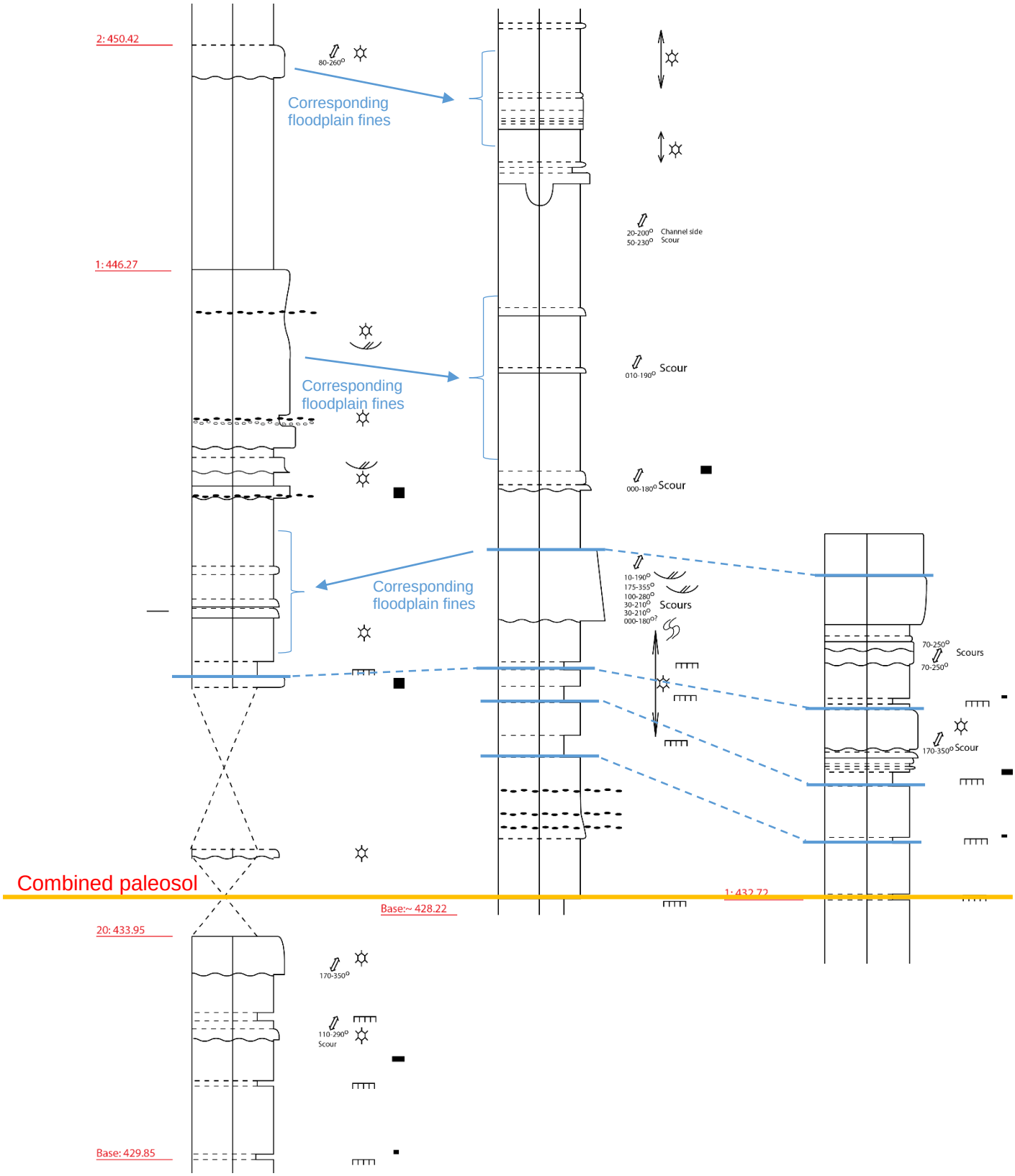

Fig. 4.5: *Option 1: A combination of the paleosol 1 and the paleosol in butte 2 with an azimuth of 269˚ and a dip of 0.57˚ was used to calculate the expected heights. These heights were plotted in the logs of butte 1&2 and the log of the base of the Marcén ridge.*

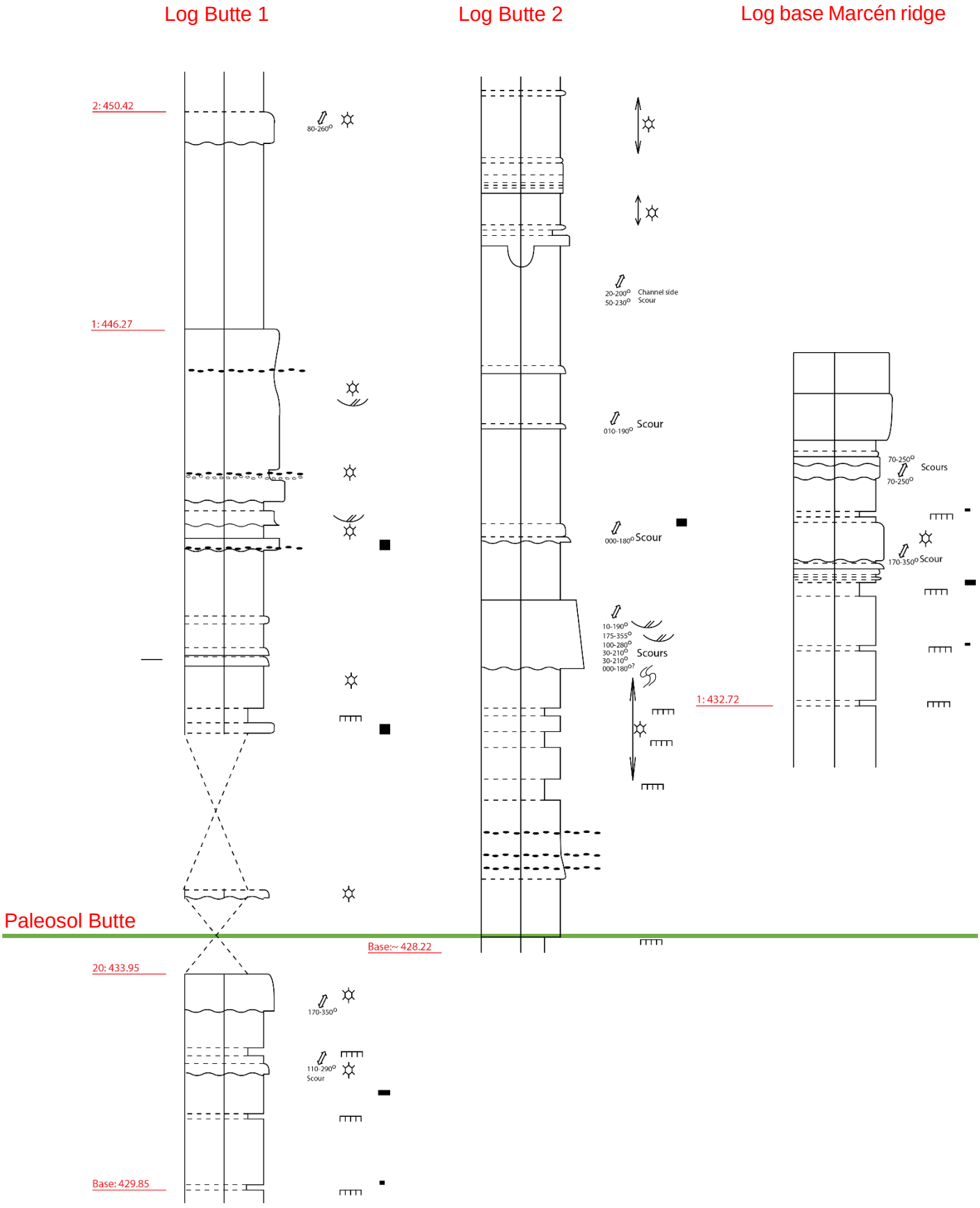

Fig. 4.6: *Option 2: The expected height of the paleosol in butte 2 plotted in the logs of butte 1&2 and the log of the base of the Marcén ridge. An azimuth of 302˚ and a dip of 0.53˚ was used to calculate these expected heights*

4.3 3D Modelling

A 3D model of the Marcén ridge was developed and can be seen in Fig. 4.6. This model was supposed to be used for correlating the sandstone bodies along the ridge together with the azimuth and dip of the paleosols. The 3D model turned out well enough for analysing but a program that allows to draw planes through the model and is able to handle the size of the file still needs to be found. This meant that at this moment it is impossible to retrieve accurate information from the model.

4.4 Lateral Net-to-Gross ratio

To be able to say something about the reservoir potential of fluvial deposits without the 3D model, a 2D analysis with the help of photo panels of the net-to-gross ratio was performed. In these photo panels, a distinction was made between the channel sand deposits (yellow) and the floodplain deposits (blue). (Fig 5.7)

When comparing the lateral net-to-gross ratio along the ridge it is evident that this ratio is laterally heterogeneous. Virtual wells A, B and C have been drawn in the figure to compare the ratio along the ridge. Looking at wells A and C large sand bodies with some thinner layers in between can be observed. The net-to-gross ratio has a value of approximately 0.55. Following the well path of B only thin sands can be recognized with larger vertical spacing in between. This well has a net-to-gross ratio of about 0.3. When looking for the boundaries of the low and high net-to-gross regions we can observe them in the ESE part of panel b. and c. This is a sharp transition of large, thick sand bodies to thinner, smaller sands.

Another matter that stands out when looking at the distribution of channel and floodplain deposits relative to each other, is that the floodplain deposits always appear below a sand body. The floodplain deposits never seem to appear as individual deposits, while sand layers are found by themselves

Fig. 4.7: *The 3D model made with Agisoft photoscan. The shape and structure of the ridge and its fluvial deposits can be seen. Flags represent the dGPS marker points used to georeference the model. The ridge is 2.25km long and 150m high.*

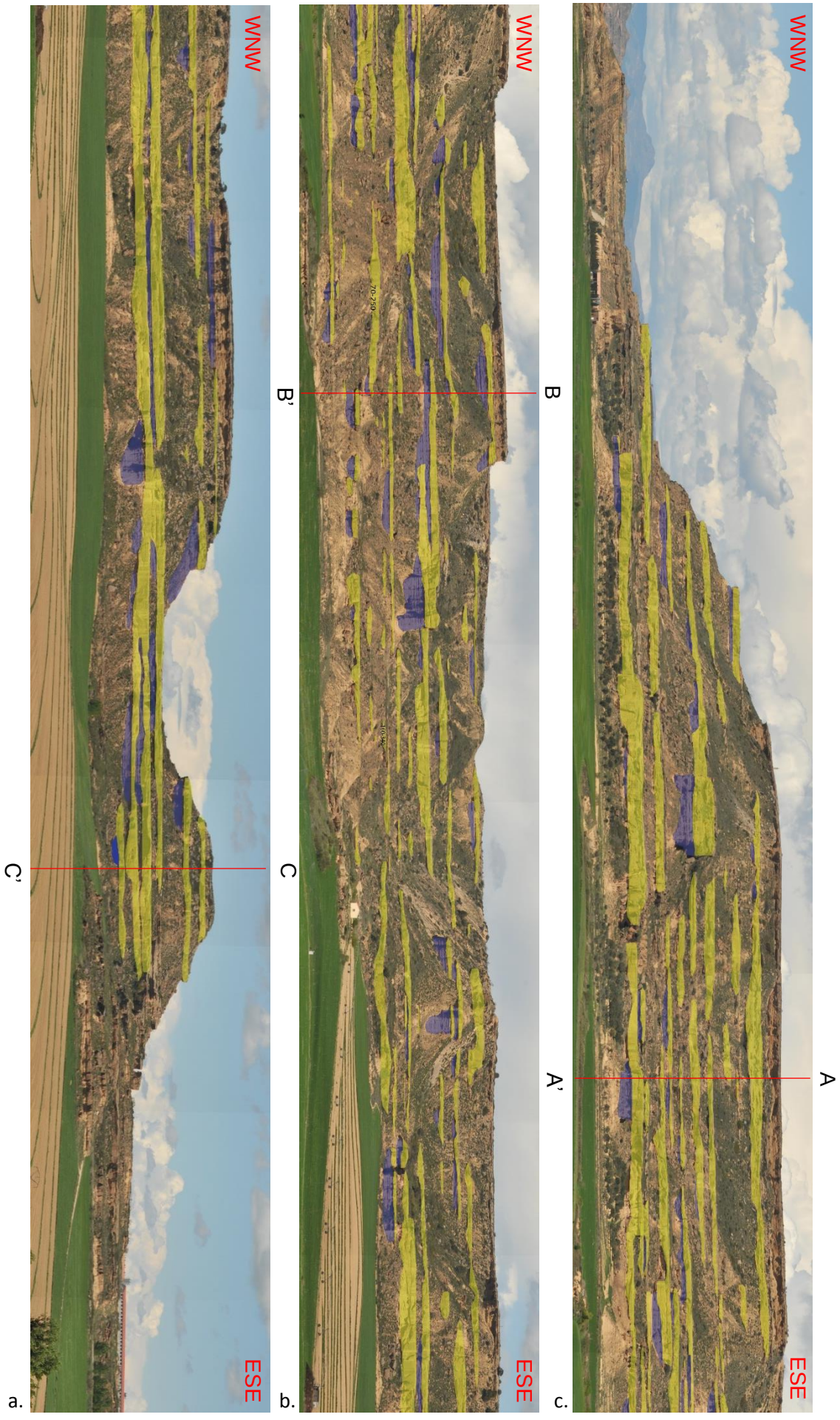

Fig. 4.8: *The Marcén ridge with indicated sandstone channel deposits (yellow) and floodplain deposits (blue). A, B and C represent virtual well paths. Comparing the net-to-gross ratio at these wells shows that fluvial deposits are laterally heterogeneous. Enlarged panels can be found in Appendix C*

5. Discussion

5.1 Floodplain morphology

For the determination of the azimuth and dip of the paleosol in the lower region of the Marcén ridge the combination of the paleosol in butte 2 and the base of the ridge have been chosen over the values for the paleosol in butte 2. Despite the high R^2 value of paleosol butte 2 and a sensitivity analysis that shows the calculation is accurate the decision was made that the combination gave a better approximation of the whole area. However, this does not mean the accurate measurements are neglected. For the vicinity of butte 2, the paleosol will have the calculated azimuth and dip. This local deviation may be caused by the floodplain not being perfectly flat and horizontal at the moment of formation. This effect originates from topographic variability of the floodplain due to irregular spatial deposition of floodplain deposits. (Leclerc & Hickin,1997) This can result in local variations of the azimuth and dip in a studied area but to correlate the whole area average values need to be used for log correlation.
The sensitivity analysis of the combined paleosol shows histograms with a bimodal distribution when n=6. This can be explained by the fact that there are eighteen data points from butte 2 and five from paleosol 1. The chance that the randomly selected values only contain data points from the butte is large and subsequently a bimodal distribution forms. To solve this a larger number of random values was selected and this resulted in more constant values.

5.2 Well log correlation

From the results of this study, conditions can be composed for essential information that needs to be retrieved from cores and logs to correlate between wells. A first necessity is one or more paleosols or a sharp boundary to level the lithostratigraphic logs on. The problem with paleosols is that their spatial distribution might not be extensive enough to cover the distance between wells. In a fluvial system channel deposits may show little evidence of pedogenesis because sedimentation near the main river channel is rapid. Overbank deposition is slow and the deposits tend to thin and decrease in grain size the further distal from the active channel. This means there is less sediment influx further away from the channel and as a result, paleosol development will only occur distal from the main active channel and may therefore not be spatially continuous. (Kraus, 1999) Even in the studied area, some paleosols cannot be followed in the logs. Another issue with paleosols is that cored intervals of the deposits are needed to be able to recognize them. Many production wells only have logs available and if there are cores this mostly is of the primary target interval. Fluvial deposits are a secondary target, and therefore core samples of that interval are often not produced. In the case that cores are available, together with the information from FMI/FMS logs, valuable data about the flow directions of the main channel can be retrieved. In a low sinuous fluvial system this can help predict the main channel direction and help to correlate sandstone bodies and floodplain deposits in logs. If only logs are available sharp boundaries like the primary reservoir target or the seal can also serve as a correlation horizon.

5.3 Distribution of channel and floodplain deposits

A feature that stood out during analysis was that floodplain deposits were always found covered by channel sands. There are two explanations for this appearance. The first is an erosional factor where the sandstones protect the finer and weaker floodplain deposits from the elements and protect them from erosion. This would cause cliffs of floodplain deposits covered by channel sand bodies. The second explanation for this feature is that crevasse splays create an opportunity for the main channel to avulse into the channels of the crevasse splay. During a period of flooding, the levees break and crevasse splays form and after various floods stacked crevasse deposits form (Donselaar et al., 2015). When a crevasse splay forms, shallow unstable channels develop quickly as the splay enlarges. With progradation and extension of the splay margins, channelization becomes more pronounced. As the splay enlarges it becomes more elongate, and eventually the extending channels begin to flow subparallel to the main channel following the regional slope. Many of the developing crevasse channels join to form an anastomosing pattern aggrading the floodplain, and this will continue until there is no more uninvaded floodplain available. (Mohrig et al., 2000) To be able to handle the sediment load, channels will become abandoned and flow becomes concentrated in fewer but larger channels. Whenever flow is diverted away from its main

channel, it will seek the path of highest gradient or greatest flow efficiency. (Slingerland & Smith, 2004) The end result is a single channel following the regional gradient that will cause an avulsion of the main channel. The avulsion may happen rapidly during one single flood event or more gradually over a longer period of time where anastomosing channels are active. When the anastomosing channel are all merged into a single river channel, portions of the previously deposited crevasse splays will be incised by the newly formed river channel. The process is depicted in Fig. 5.1. (Smith et al., 1989)

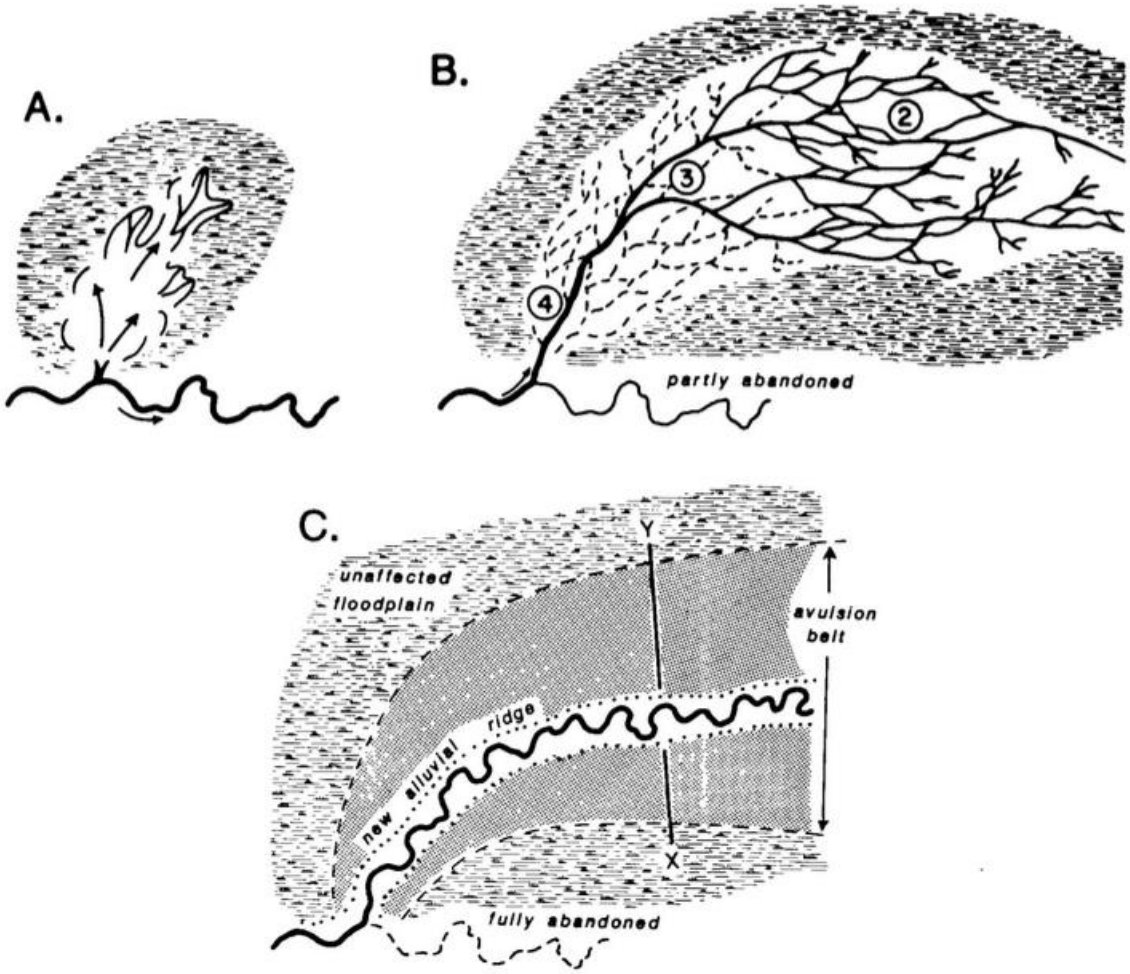

Fig. 5.1: *Sketches of an avulsion triggered by crevasse splays. (A) Crevasse splays form during a period of flooding, forming small, unstable channels. (B) As the progadation of the crevasse complex continues, the floodplain is invaded and an anastomosing system forms. When the floodplain is filled fewer but larger channels start to form while others are abandoned. Partial avulsion is the result. (C) The original channel is now fully abandoned since the avulsed channel has a higher gradient. Modified from Smith et al., 1989.*

Channels incising and overlying floodplain deposits were observed in the Marcén ridge. This can be seen in Fig. 4.8 where all three panels show blue floodplain deposits covered by channel sands. Another explanation for this feature is a combination of both previously stated possibilities. Crevasse splay development can be a reason for a channel to avulse but because of the stacking of channel sands onto floodplain deposits the whole sequence is well preserved. If floodplain deposits do not have a stronger layer laying over them they are more exposed to weathering and less of the deposits will be preserved in outcrops.

5.4 Channel nesting

The lateral heterogeneity of the fluvial systems can be explained by the previously described process of avulsion. The Huesca Fluvial system is sandy and would thus be splay-prone. (*sensu* Jones & Hayek 2007) Splay-prone systems are likely to form transitional avulsions which are characterized by a stratigraphy where channel sands are overlying crevasse splays and floodplain deposits. (Noordijk, 2014) The previously described avulsions triggered by crevasse splays in 5.3 are described by Mohrig et al. (2000) as an

aggradational avulsion model. In this model many the anastomosing channels feed back into the main channel possibly via a pre-existing tributary. Eventually a single channel forms of sufficient flow depth to scour into the underlying aggradational floodplain deposits. This model causes a local avulsion. After a period of aggradation of the new channel the same process will repeat itself. (Mohrig et al., 2000)

Anastomosis is likely to be a part of a transitional pattern forced by the need to handle the increased sediment load during a flooding event. When the low areas of the floodplain are aggraded the flow will be captured in a single-thread channel. In this case, the aggradational avulsion model is in time a product of small local avulsions hierarchically superimposed by a regional avulsion. (Slingerland & Smith, 2004)
An avulsion can also reoccupy an abandoned channel, which is called avulsion by annexation (*sensu* Jones & Hayek, 2007*)*. There are several possible explanations. The abandoned channel can form a topographical low after a period of aggradation of the newly avulsed channel or the avulsed channel can be either bigger or smaller which can make it more flow efficient to reside into an old channel. In this scenario either two channel sands can be found on top of each other or floodplain deposits are wedged between two channel sands. This can be observed in both section a. and the lower region of section c. of Fig 4.8 where stacked channel sands and wedged floodplain deposits can be found.
Either the aggradational avulsion model or avulsion by annexation, as well as a combination of the two theories can explain the heterogeneous lateral net-to-gross ratio along the Marcén ridge. The aggradational avulsion model would explain the transitional avulsions where channel sands overly flood plain deposits and the avulsion by annexation would explain the succession of channel sands and wedged floodplain deposits. The combination of theories causes a stacked, nested succession of channel and floodplain deposits in the outcrop until a regional avulsion of the channel belt will occur, but more research on this topic is needed to prove this theory.

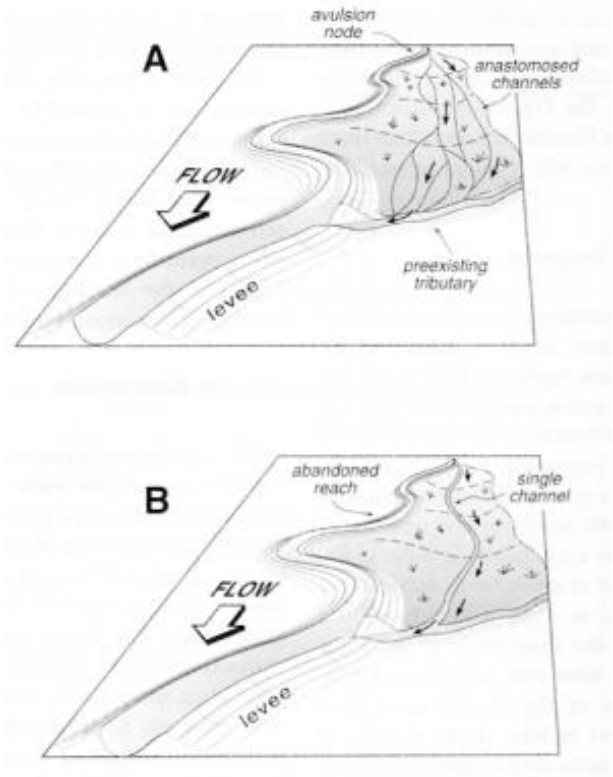

Fig. 6: *Schematic view of an aggradational avulsion model. (A) early stage where the avulsion is flowing out along the floodplain. Rapid aggradation forms anastomosing channels that fill the topographic lows of the floodplain during the flood event. (B) A single flow has formed eroding the aggradational deposits, and the avulsion is complete. From Mohrig et al., 2000*

5.5 Reservoir potential

The laterally heterogeneous net-to-gross ratio of the Marcén ridge can have major implications on the reservoir potential of comparable fluvial deposits. The difference along the ridge becomes evident when comparing the virtual well paths in Fig. 4.8. The reservoir potential and net-to-gross ratio of well A and well C are desirable while well B has a considerably lower net-to-gross ratio. This difference is about 0.2 when looking at the net-to-gross ratio. The reservoir potential of such deposits is dependent on the connectivity between the different parts of the reservoir. If for example crevasse splays connect the high net-to-gross parts with the low net-to-gross part the volume to be produced from one well increases substantially. However, crevasse splays do have a permeability in the sub-mD region which can cause problems when hydrocarbons have to flow through these sands. A high reservoir pressure is needed or more permeability has to be created. The heterogeneity of the ridge has an impact on reservoir modelling because the information retrieved from well log data cannot be applied to the whole reservoir. As the transitions in net-to-gross ratio are abrupt, the information retrieved from two wells drilled 50m apart can differ considerably. This makes a prediction on reservoir volume difficult. It cannot be known with data from one well if one has drilled into the higher or lower net-to-gross regions as there is no comparison available concerning that particular fluvial system in the subsurface.

6. Conclusion

This study of the fluvial deposits of the Marcén ridge provided input for a deterministic reservoir model that predicts correlation lengths, nesting and reservoir potential of thin-bedded fluvial reservoir sandstone in an overall low net-to-gross setting.
Correlation lengths between wells are dependent on the spatial distribution of a correlation horizon. This horizon can be one or more paleosols, but spatial distribution of paleosols in a fluvial system may not be extensive enough to cover the distance between wells. In well logs, sharp sequence boundaries can also be used as a correlation horizon.
Nesting of river channels can give an explanation about the origin of the lateral heterogeneous distribution of sand bodies. This nesting can be caused by local avulsions of the river channel triggered by flood events and crevasse splay formation. When a crevasse forms, it forms channels and extends into the floodplain. As the splay enlarges it forms an anastomosing pattern that aggrades the floodplain until there is no more local uninvaded floodplain available. The flow will become concentrated into increasingly fewer and larger channels and will eventually result in one single channel. Flow will than seek the path of highest gradient or greatest flow efficiency. Avulsion by annexation, where a channel reoccupies an old channel, can give a second explanation for the nesting. After a period of time it can be more flow efficient to directly flow through the old channel again. A combination of the two explanations can provide a theory for the nesting of river channels. Local avulsions, together with re-occupation of river channels will cause the river to flow in a restricted space and can cause the lateral heterogeneity in net-to-gross ratio. More research is needed to support this theory.
The laterally heterogeneous character of the Marcén ridge can have major implications on reservoir potential. The potential is dependent on the connectivity between the higher and lower net-to-gross regions by for example crevasse splays. Even if they are connected crevasse splays do have a permeability in the sub-mD region which can cause problems when hydrocarbons have to flow through these sands. A high reservoir pressure is needed or more permeability has to be created. The heterogeneity also has an impact on reservoir modelling as there only is a limited subsurface expression from wells. Therefore, it cannot be known if one is looking at the higher or lower net-to-gross zones for that particular fluvial system which makes estimates about reservoir volume difficult and inaccurate.

Most methods used to acquire and process data have proven to be useful tools. dGPS measurements are a precise and efficient method to measure spatial data in regions with a minimal tectonic dip. Next to this, the measurements have also proven useful for georeferencing the logs and the stereographic projection. Photo panels are accurate enough give an indication about the main structures and transitions of fluvial sediments. The 3D modelling software gave a reasonable output but could not be used for accurate analysing.

7. Recommendations

- A study of the paleosols in the Huesca Fluvial fan is necessary to be able to determine the spatial distribution throughout the fan. In this study the interpretation of the paleosols was based on colour, but more aspects can be documented to be able to follow the paleosols over a larger area.

- dGPS measurements of paleosols can be used to map the floodplain morphology at the time of deposition. Together with more detailed paleosol data this can be used to correlate larger areas of Huesca Fluvial fan.

- A program suitable for analysing the 3D model has to be found to increase the ability to correlate the Marcén ridge and other areas. It is essential that a plane corresponding to the tectonic dip can be plotted into the 3D model to be able to correlate the channel sands and floodplain deposits.

- Further research on avulsions and the potential nesting of river channels is needed. This is useful for reservoir modelling of river systems in the subsurface because more can be said about the development of a river system. This will improve the accuracy of reservoir models.

- More research on connectivity between low and high net-to-gross zones is necessary. If these regions are connected by crevasses splays, reservoir volume and potential greatly increase.

- More research on correlation horizons in fluvial depositional systems in well logs and cores is needed to be able to say something about the spatial extensiveness of such horizons. Such a study will provide more detailed information about correlation lengths between wells.

List of references

1. Donselaar, M.E., Bouman, L., Noordijk, N., Toorenenburg, K.A. van & Weltje, GJ (2015). Reservoir potential of thin-bedded sandstone in continental mudrock successions - The search for hidden treasures. In M Mozetic (Ed.), *Proceedings of the 77th EAGE conference and exhibition, 2015* (pp. 3647-3651). Houten: EAGE.

2. Donselaar, M.E., Schmidt, J.M. (2005). Integration of outcrop and borehole image logs for high-resolution facies interpretation: example from a fluvial fan in the Ebro Basin, Spain. *Sedimentology,**52**, 1021-1042.*

3. ECORS Pyrenees Team (1988). The ECORS deep reflection seismic survey across the Pyrenees. *Nature*, **331**, 508–510.

4. Hirst, J.P.P. (1992). Variations in alluvial architecture across the Oligo-Miocene Huesca fluvial system, Ebro Basin, Spain. *CSP3 (SEPM),* 111-121.

5. Jones, H. and Hajek, E. (2007). Characterizing avulsion stratigraphy in ancient alluvial deposits. *Sedimentary Geology*, **202**:124–137.

6. Kraus, M. J. (1999). Paleosols in clastic sedimentary rocks: their geologic applications. *Earth-Science Reviews*, **47**,41–70.

7. Li, J., Donselaar, M.E., Hosseini Aria, S.E., Koenders, R., Oyen, A.M. (2014). Landsat imagery-based visualisation of the geomorphological development at the terminus of a dryland river system. *Quaternary International*, **352**, 100-110.

8. Li, Y., Ruichek, Y., Cappelle, C. (2011, Oct 5-7). *3D triangulation based extrinsic calibration between a stereo vision system and a LIDAR.* Paper presented at the 2011 14th International IEEE Conference on Intelligent Transportation Systems (ITSC). DOI: 10.1109/ITSC.2011.6082899

9. Leclerc, R.F., Hickin, R.J. (1997) The internal structure of scrolled floodplain deposits based on ground-penetrating radar, North Thompson River, British Columbia. *Geomorphology,* **21**, 17-38.

10. Lloyd, M.J., Nichols, G.J., Friend, P.F. (1998). Oligo-Miocene alluvial-fan evolution at the southern Pyrenean thrust front, Spain. *Journal of Sedimentary Research*, **68**, 869-878.

11. Mohrig, D. and Heller, P. (2000). Interpreting avulsion process from ancient alluvial sequences: Guadalope-Matarranya system (northern Spain) and Wasatch Formation (western Colorado). *Geological Society of America Bulletin*, **12,**1787–1803.

12. Noordijk, N. (2014) Geological characterization of thin-bedded crevasse splay sandstones; outcrop-analogue studies for tough gas reservoir potential. Master's Thesis, Delft University of technology. Retrieved from: uuid:ab901b88-a16d-4c0c-975a-535bc3f84662

13. Nichols, G. and Fisher, J. (2007). Processes, facies and architecture of fluvial distributary system deposits. *Sedimentary Geology*, **195**, 75–90.

14. Puigdefàbregas, C., Muñoz, J.A., Vergés, J. (1992). Thrusting and foreland basin evolution in the southern Pyrenees. *Thrust tectonics,* 247-254.

15. Slingerland, R., Smith, N.D. (2004) River avulsions and their deposits. *Annu. Rev. Earth Planet. Sci*. **32,** 257–285.

16. Smith, N.D., Cross, T.A., Dufficy, J.P., Clough, S.R. (1989) Anatomy of an avulsion. *Sedimentology,* **36,** 1-23.

17. Toorenenburg, K.A. van, Donselaar, M.E., Weltje, G.J. (2015). Reservoir architecture and tough gas reservoir potential of fluvial crevasse-splay deposits. In M Mozetic (Ed.), *Proceedings of the 77th EAGE Conference and Exhibition, 2015* (pp. 2317-2321). Houten: EAGE.

18. Weltje, G.J., Ansenwoude, S.O.K.J. van, Boer, P.J. de (1996). High-frequency detrital signals in Eocene fan-delta sandstones of mixed parentage (southcentral Pyrenees, Spain): a reconstruction of chemical weathering in transit. *Journal of Sedimentary Research*, **66**, 119–131.

Appendices

Appendix A: dGPS measurements of the paleosols in ETRS89 UTM coordinates

Paleosol 3	UTM Northing	UTM Easting	Height (m)
	4645280.9	726744.8	457.8898
	4645279.1	726697.1	457.5704
	4645282.3	726693	457.533
	4645307.1	726665.6	457.1413
	4645313.1	726612.9	456.7096
	4645322.6	726608.9	456.5838
	4645364.9	726526.3	456.1447
	4645362.8	726516.1	456.0561
	4645287.7	726796.1	458.1774
	4645289.4	726782.4	458.2326
	4645179.4	726816.2	458.5018
	4645179.7	726827.3	458.3592
	4645180.1	726840.3	458.7004
	4645180.4	726848.3	458.9488
	4645182.1	726901.1	458.9290
	4645182.1	726903.5	459.0795
	4645182.5	726913.5	458.8658
	4542364.9	730172.8	458.9263
	4542364.7	730166.5	458.7705
	4542364.6	730163.3	458.6076
	4542365.9	730204.4	459.0435
	4542366	730207.1	458.8839
	4542366.3	730217.8	459.0020
	4542366.6	730226.2	459.1623
	4542366.6	730228	459.3702
	4542367.1	730241.9	459.5149
	4542367.8	730265	459.4825
	4542367.9	730268.9	459.5645
	4542368.4	730282.7	459.6672
	4542369.3	730311.8	459.7813
	4542369.4	730316.7	459.7965
	4542369.2	730308.3	460.2387
	4645274.9	726704.2	457.6928
	4645378.4	726516.3	455.8974
	4645411	726405.3	454.8763
	4645405.2	726386.8	454.5346
	4645412.4	726367.8	455.0937
	4645376.3	726545.4	456.0965

Paleosol 2	UTM Northing	UTM Easting	Height (m)
	4645566.8	725973.8	452.06
	4645642.3	725899.6	451.6791
	4645650.4	725836.7	451.3967
	4645676.7	725828.8	451.0148
	4645757.2	725764.8	450.8632
	4645747.9	725757.2	450.7581
	4645730.8	725747.8	450.7624
	4645726.1	725739.3	450.607
	4645674.5	725652	450.6439
	4645631.8	725885.4	451.8582

Paleosol 1	UTM Northing	UTM Easting	Height (m)
	4645090.2	726636	432.9881
	4645083.4	726628	432.922
	4645085.4	726621.2	432.8703
	4645100.8	726719.1	432.8713
	4645087.4	726732.7	433.067

Paleosol Butte 2	UTM Northing	UTM Easting	Height (m)
	4643868.9	726248.4	428.6977
	4643877.9	726236.4	428.5975
	4643880.1	726228.5	428.4768
	4643882.2	726207.7	428.392
	4643880.5	726196.4	428.3167
	4643885.9	726171.1	428.1466
	4643941.9	726128	427.5338
	4643969	726126.3	427.3871
	4643989.1	726125.5	427.2435
	4644008	726140.7	427.2285
	4644002.9	726165.3	427.5265
	4643996.1	726182.8	427.5744
	4643994.6	726204.9	427.7983
	4643992	726228.3	427.9939
	4643984.8	726246.9	428.1346
	4643848.5	726268	429.0078
	4643896.9	726387	429.7592
	4643847.4	726369.8	429.9296

Appendix B: Lithostratigraphic logs

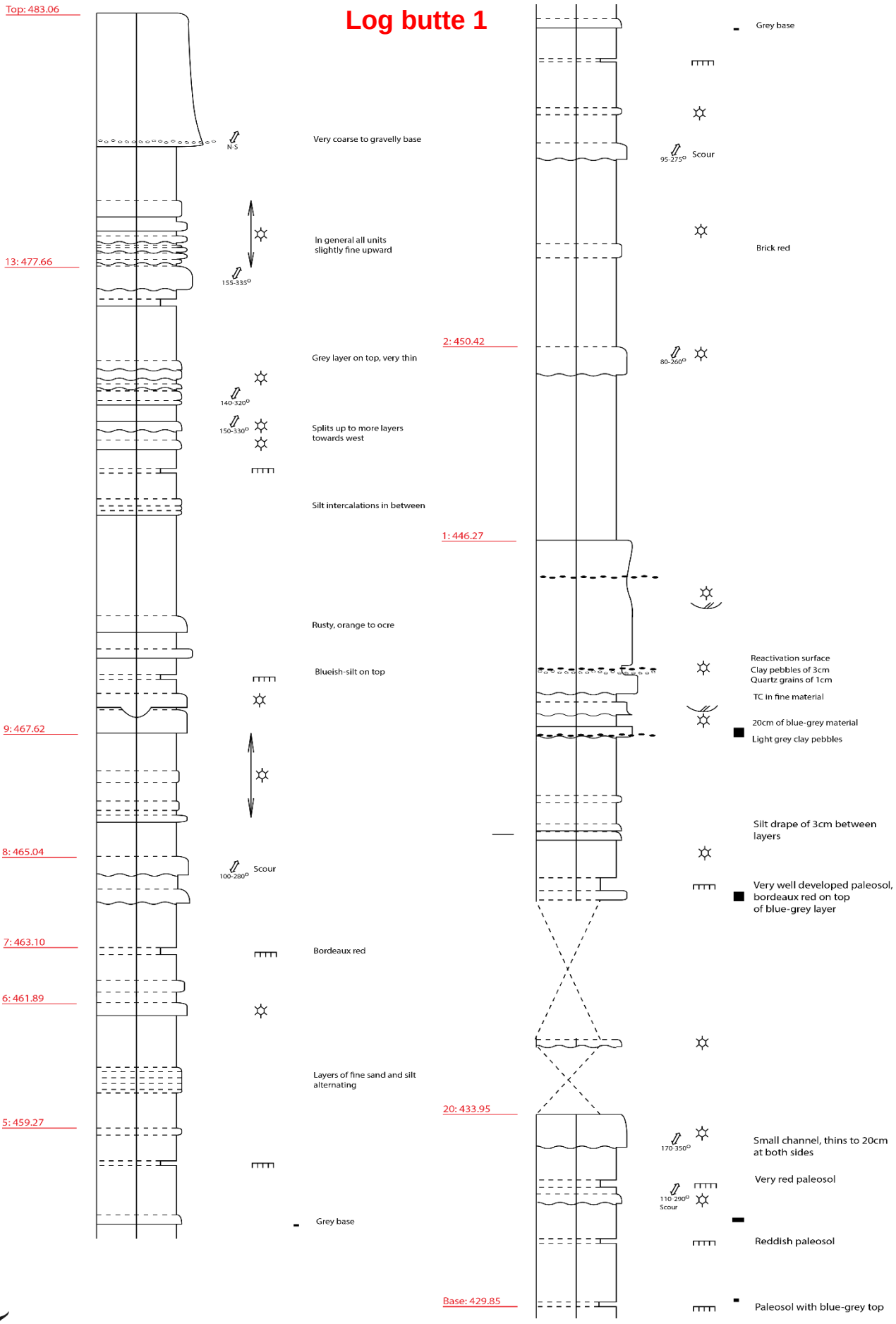

Log butte 2

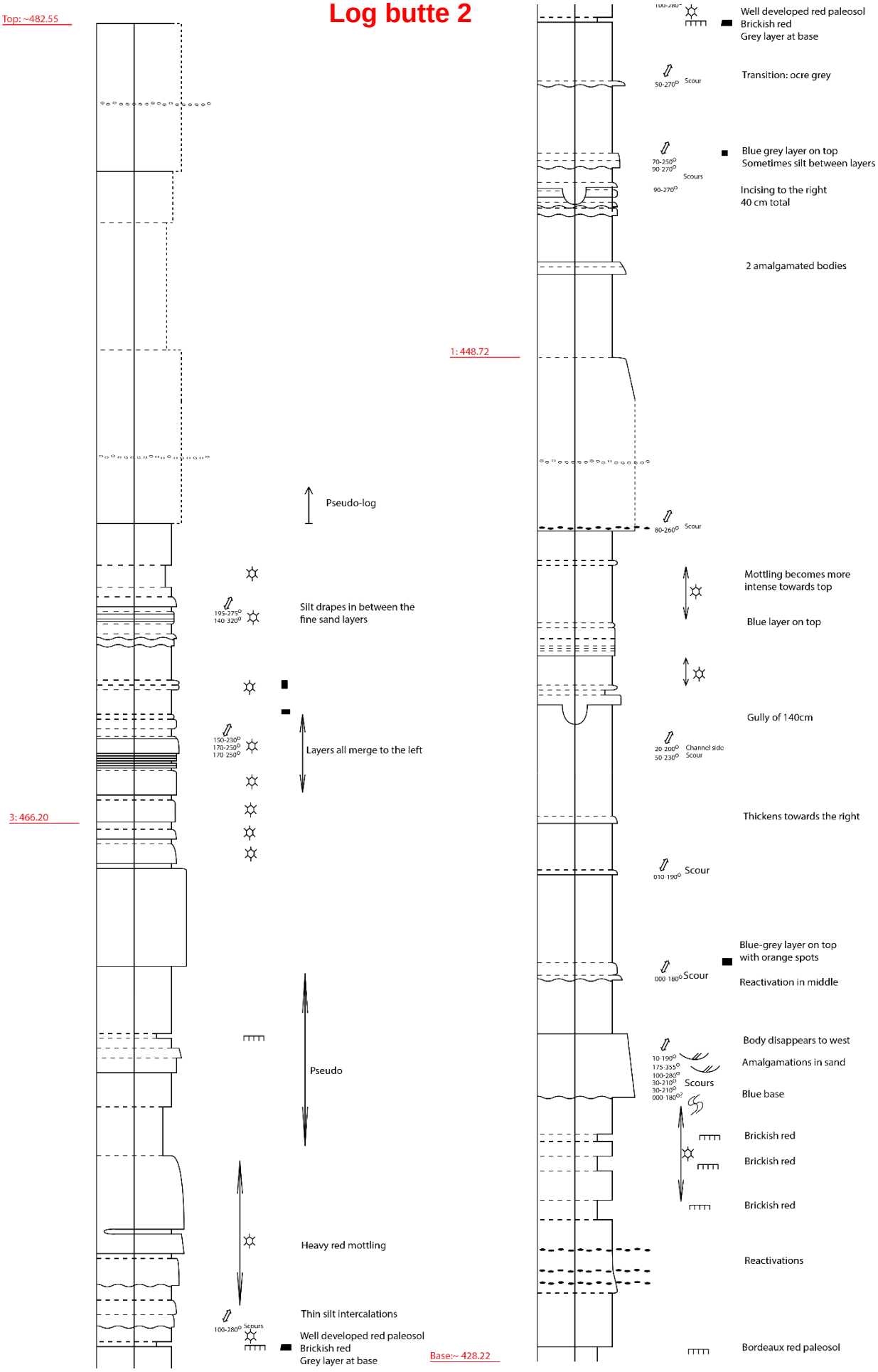
Top: ~482.55
3: 466.20
1: 448.72
Base:~ 428.22
Pseudo-log
195-275°
140-320°
Silt drapes in between the fine sand layers
150-230°
170-250°
170-250°
Layers all merge to the left
Pseudo
Heavy red mottling
100-280°
Scours
Thin silt intercalations
Well developed red paleosol
Brickish red
Grey layer at base
Well developed red paleosol
Brickish red
Grey layer at base
50-270°
Scour
Transition: ocre grey
70-250°
90-270°
Scours
90-270°
Blue grey layer on top
Sometimes silt between layers
Incising to the right
40 cm total
2 amalgamated bodies
80-260°
Scour
Mottling becomes more intense towards top
Blue layer on top
Gully of 140cm
20-200°
50-230°
Channel side
Scour
Thickens towards the right
010-190°
Scour
000-180°
Scour
Blue-grey layer on top
with orange spots
Reactivation in middle
10-190°
175-355°
100-280°
30-210°
30-210°
000-180°?
Scours
Body disappears to west
Amalgamations in sand
Blue base
Brickish red
Brickish red
Brickish red
Reactivations
Bordeaux red paleosol

Log 4

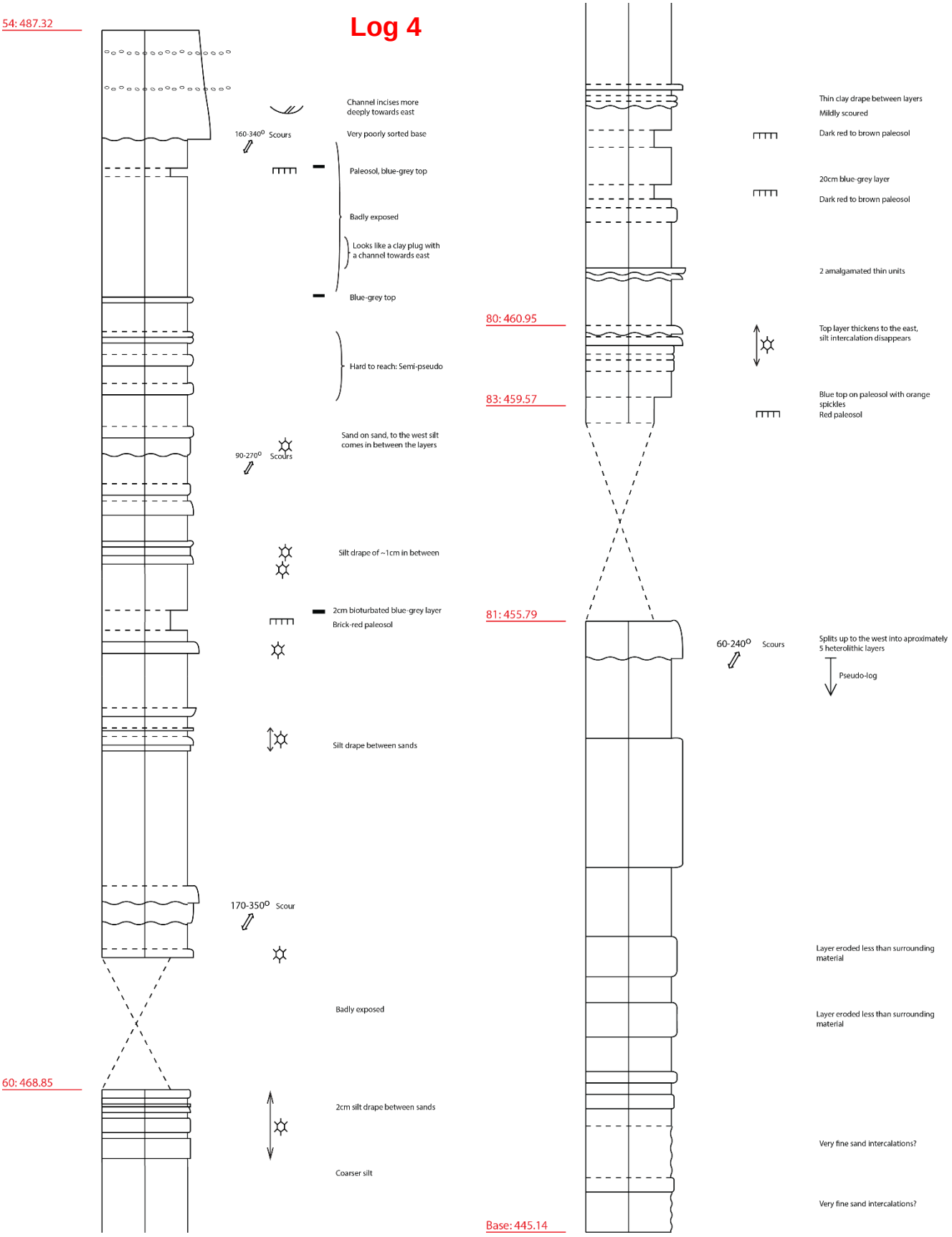
54: 487.32
Channel incises more deeply towards east
160-340° Scours
Very poorly sorted base
Paleosol, blue-grey top
Badly exposed
Looks like a clay plug with a channel towards east
Blue-grey top
Hard to reach: Semi-pseudo
Sand on sand, to the west silt comes in between the layers
90-270° Scours
Silt drape of ~1cm in between
2cm bioturbated blue-grey layer
Brick-red paleosol
Silt drape between sands
170-350° Scour
Badly exposed
60: 468.85
2cm silt drape between sands
Coarser silt
Thin clay drape between layers
Mildly scoured
Dark red to brown paleosol
20cm blue-grey layer
Dark red to brown paleosol
2 amalgamated thin units
80: 460.95
Top layer thickens to the east, silt intercalation disappears
83: 459.57
Blue top on paleosol with orange spickles
Red paleosol
81: 455.79
60-240° Scours
Splits up to the west into aproximately 5 heterolithic layers
Pseudo-log
Layer eroded less than surrounding material
Layer eroded less than surrounding material
Very fine sand intercalations?
Very fine sand intercalations?
Base: 445.14

Log 6

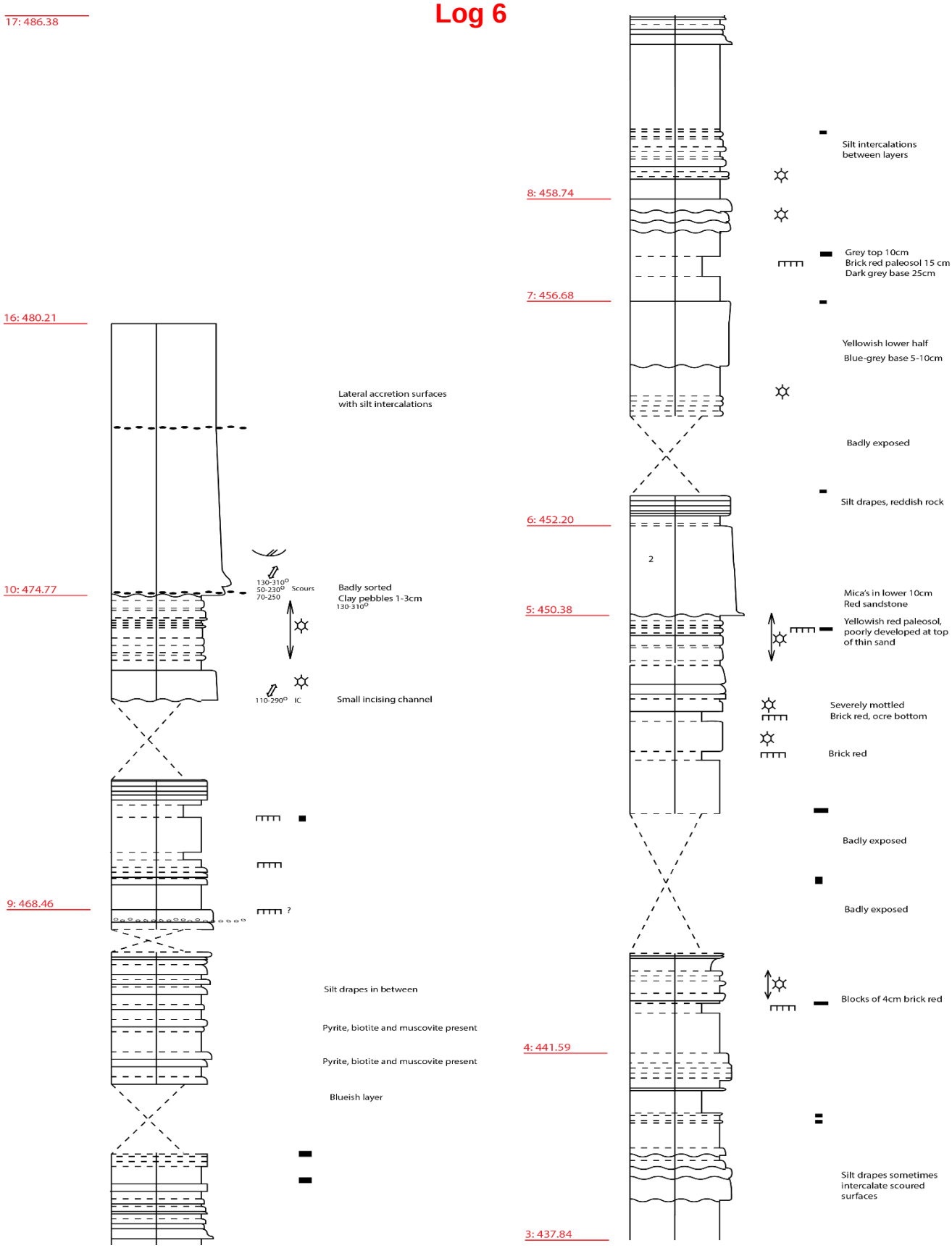
17: 486.38
16: 480.21
10: 474.77
9: 468.46
8: 458.74
7: 456.68
6: 452.20
5: 450.38
4: 441.59
3: 437.84
Lateral accretion surfaces with silt intercalations
130-310°
50-230°
70-250
Scours
Badly sorted
Clay pebbles 1-3cm
130-310°
110-290°
IC
Small incising channel
?
Silt drapes in between
Pyrite, biotite and muscovite present
Pyrite, biotite and muscovite present
Blueish layer
Silt intercalations between layers
Grey top 10cm
Brick red paleosol 15 cm
Dark grey base 25cm
Yellowish lower half
Blue-grey base 5-10cm
Badly exposed
Silt drapes, reddish rock
2
Mica's in lower 10cm
Red sandstone
Yellowish red paleosol, poorly developed at top of thin sand
Severely mottled
Brick red, ocre bottom
Brick red
Badly exposed
Badly exposed
Blocks of 4cm brick red
Silt drapes sometimes intercalate scoured surfaces

Log base Marcén ridge

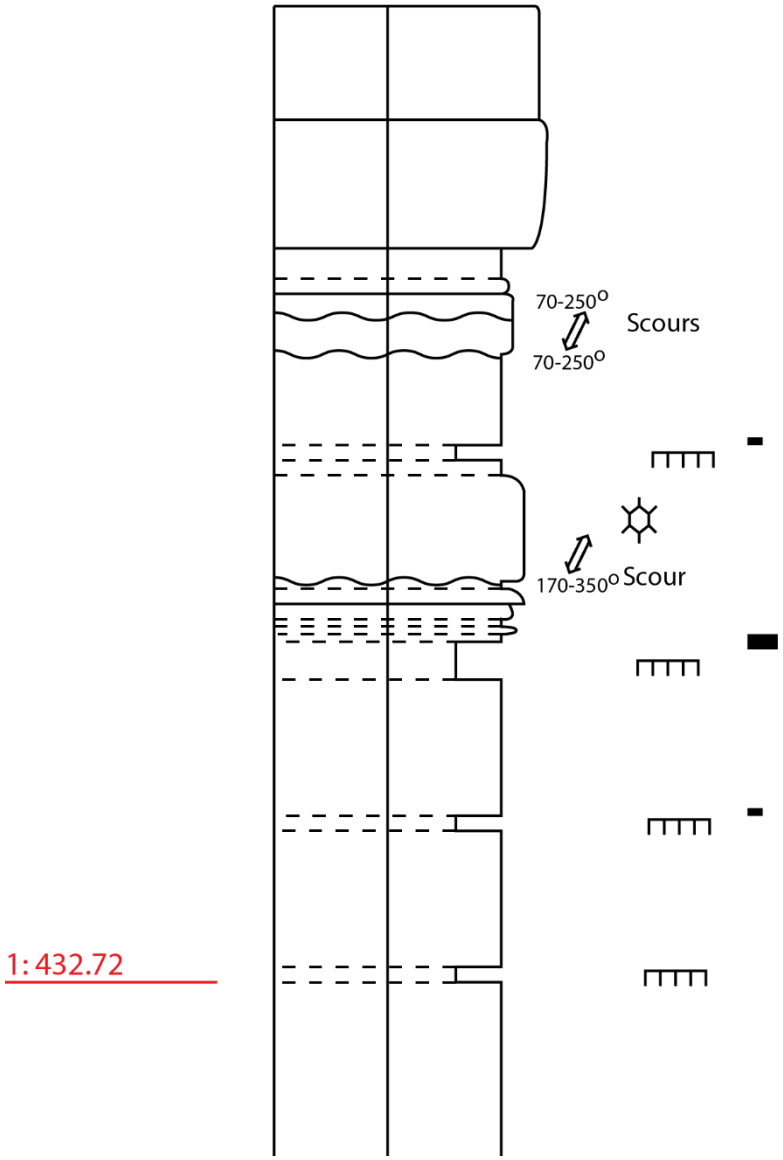

Appendix C: Photo panels

A

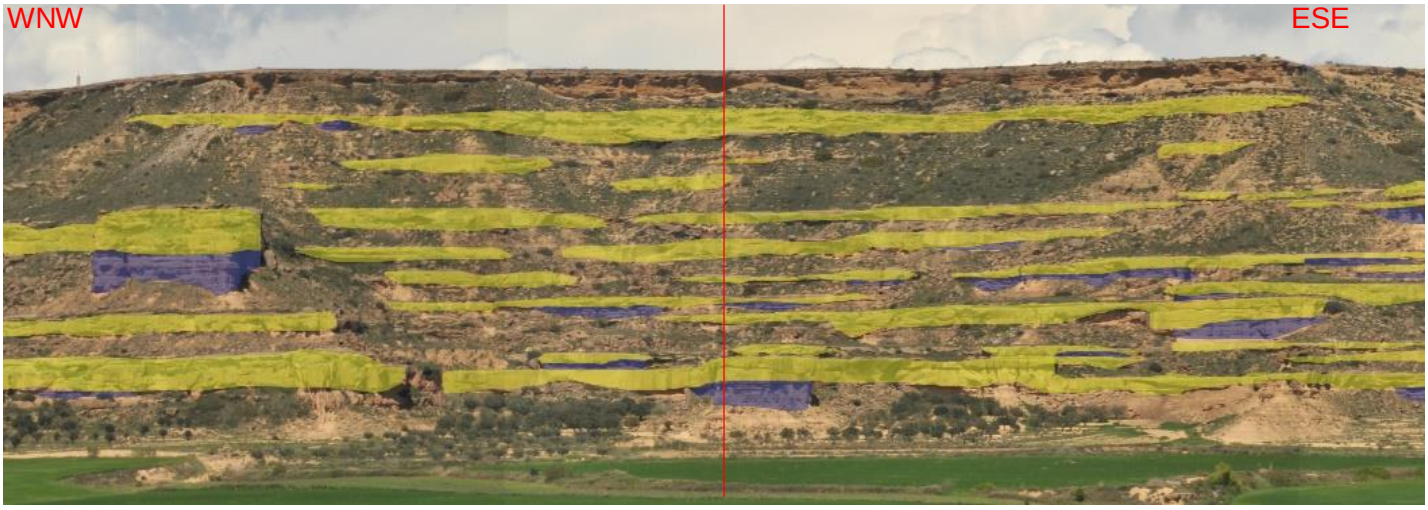

A’

B

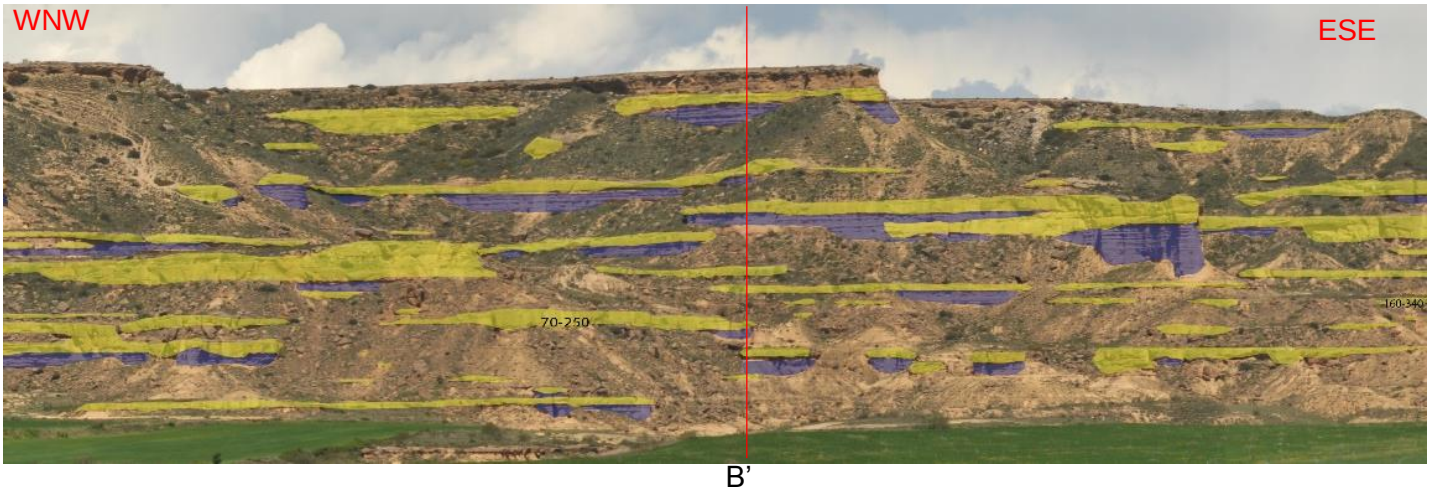

B’

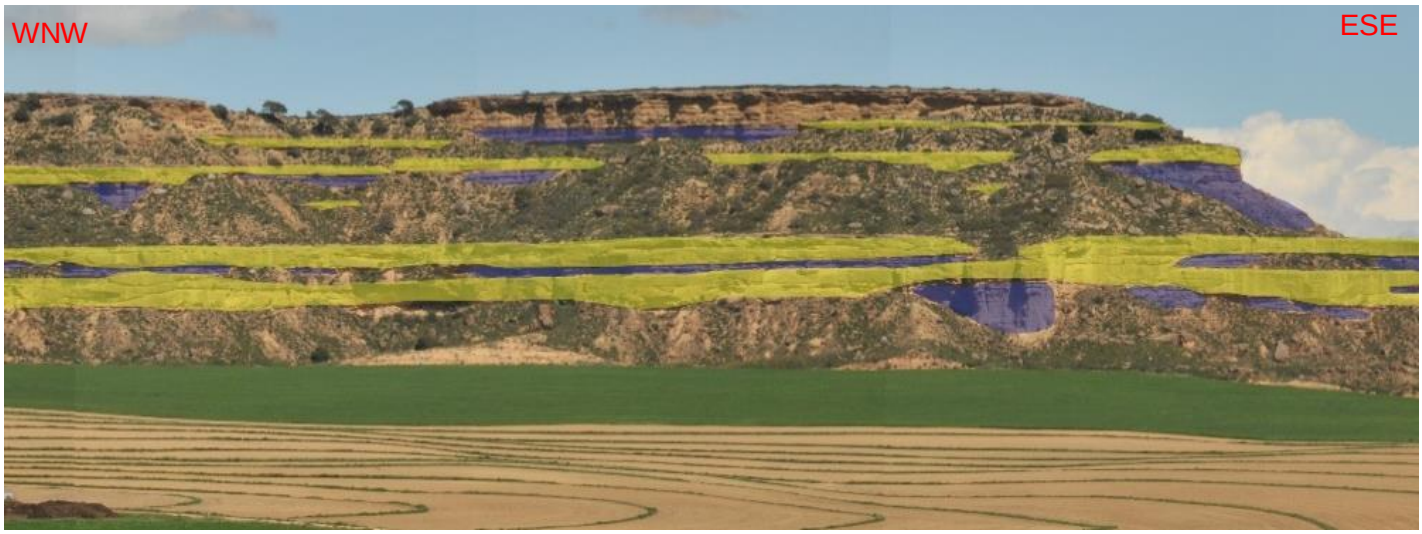

C

C’